

A novel higher-order numerical method for parabolic integro-fractional differential equations based on wavelets and $L2-1_\sigma$ scheme.

Sudarshan Santra^a and Ratikanta Behera^{a*}

^aDepartment of Computational and Data Sciences, Indian Institute of Science, Bangalore, India

ABSTRACT

This paper aims to construct an efficient and highly accurate numerical method to solve a class of parabolic integro-fractional differential equations, which is based on wavelets and $L2-1_\sigma$ scheme; specifically, the Haar wavelet decomposition is used for grid adaptation and efficient computations, while the high order $L2-1_\sigma$ scheme is taken into account to discretize the time-fractional operator. In particular, second-order discretizations are used to approximate the spatial derivatives to solve the one-dimensional problem. In contrast, a repeated quadrature rule based on trapezoidal approximation is employed to discretize the integral operator. On the other hand, we use the semi-discretization of the proposed two-dimensional model based on the $L2-1_\sigma$ scheme for the fractional operator and composite trapezoidal approximation for the integral part. Then, the spatial derivatives are approximated by using the two-dimensional Haar wavelet. Here, we investigated theoretically and verified numerically the behavior of the proposed higher-order numerical method. In particular, the stability and convergence analysis of the proposed higher-order method has been studied. The obtained results are compared with some existing techniques through several graphs and tables, and it is shown that the proposed higher-order methods have better accuracy and produce less error compared with the $L1$ scheme.

KEYWORDS

Integro partial differential equation, Caputo derivative, Higher-order scheme, Haar wavelet, $L2-1_\sigma$ scheme, Error analysis.

AMS CLASSIFICATION

45K05, 45D05, 26A33, 65M06.

1. Introduction

During the past few decades, the qualitative analysis of fractional differential equations (FDEs) and fractional-order integro-differential equations (FOIDEs) have gained more popularity due to their practical application in numerous fields of science and technology, including control theory [1], cryptography [2], neural networks [3], options trading [4], and viscoelasticity [5], etc. The arbitrary order fractional derivatives, which are nonlocal in nature, are the generalized extension of the classical ones by introducing continuous Gamma functions instead of the discrete factorial functions [6]. It is also noteworthy that the singular behavior of the solution of a fractional order derivative system not only differs from the classical integer order systems but also poses a greater challenge for solving them. For a detailed study on fractional order problems having initial singularities, we direct the reader's attention to the work due to Chen *et al.* [7], Santra and Mohapatra [8]. In general, finding the analytical solution to fractional differential equations involving integral operators is impractical, since a lot of iterations are required and that makes the process more time-consuming. So one has to rely on the semi-analytical and numerical methods. A few semi-analytical approaches, such as the Adomian decomposition method [9], the homotopy analysis method [10], and the variational iteration method [11], can be used to solve FOIDEs. In addition to these, many equivalent articles are available in the literature on the numerical solutions of FDEs as well as FOIDEs based on finite

*Corresponding author. Emails: sudarshans@iisc.ac.in (S. Santra), ratikanta@iisc.ac.in (R. Behera).

difference methods [12, 13], and also on finite element methods [14]. A finite difference solution for an FDE/FOIDE at a particular time level depends on solutions at all previous time levels, however, this is not the case for integer order differential systems. Further, most of phenomena exhibit localized high frequency behavior. This makes the process more complicated, and therefore, it is mandatory to develop efficient numerical techniques to tackle fractional order systems.

Wavelet is a numerical concept that allows one to represent a function in terms of basis functions, and wavelet-based numerical methods take advantage of the fact that functions with localized regions of sharp transition are well compressed using wavelet decomposition [15, 16, 17]. This property allows local grid refinement up to an arbitrarily small scale without a drastic increase in the number of collocation points; thus, high-resolution computations can be carried out only in those regions where sharp transitions occur. It is worth mentioning that in the last few decades, the Haar wavelet method became a valuable tool for the solution of ODEs and PDEs, as well as integral and integro-differential equations, and many authors have verified it [18, 19]. Specifically, the Haar wavelet is more popular due to its beneficial properties, such as orthogonality, simple applicability, and compact support. It takes less effort and maintains accuracy for the solution and its derivatives.

The main objective of this paper is to construct and develop efficient and computationally effective numerical methods to solve the following class of time-fractional parabolic integro-partial differential equations (PDEs) of the form:

Problem I: One-dimensional integro-PDEs

$$\begin{cases} \partial_t^\alpha \mathcal{U}(x, t) - \mathcal{L}\mathcal{U}(x, t) + \mu \int_0^t \mathcal{K}(x, t - \xi) \mathcal{U}(x, \xi) d\xi = f(x, t), \\ (x, t) \in \Omega := [0, L] \times (0, T], \text{ with} \\ \mathcal{U}(x, 0) = g(x) \quad \forall x \in [0, L], \\ \mathcal{U}(0, t) = h_1(t) \text{ and } \mathcal{U}(L, t) = h_2(t) \quad \forall t \in (0, T], \end{cases} \quad (1.1)$$

Problem II: Two-dimensional integro-PDEs

$$\begin{cases} \partial_t^\alpha \mathcal{U}(x, y, t) - \mathfrak{L}\mathcal{U}(x, y, t) + \mu \int_0^t \mathcal{K}(x, y, t - \xi) \mathcal{U}(x, y, \xi) d\xi = f(x, y, t), \\ (x, y) \in \mathcal{G} := [0, 1] \times [0, 1], \quad t \in (0, T], \text{ with} \\ \mathcal{U}(x, y, 0) = g(x, y) \quad \forall (x, y) \in \mathcal{G}, \\ \mathcal{U}(0, y, t) = h_1(y, t) \text{ and } \mathcal{U}(1, y, t) = h_2(y, t) \quad \forall (y, t) \in [0, 1] \times (0, T], \\ \mathcal{U}(x, 0, t) = h_3(x, t) \text{ and } \mathcal{U}(x, 1, t) = h_4(x, t) \quad \forall (x, t) \in [0, 1] \times (0, T], \end{cases} \quad (1.2)$$

where $\alpha \in (0, 1)$. ∂_t^α denotes the fractional Caputo derivative of order α , defined by [20]:

$$\partial_t^\alpha \mathcal{U}(\cdot, t) = \left[\mathfrak{J}^{1-\alpha} \left(\frac{\partial \mathcal{U}}{\partial t} \right) \right] (\cdot, t) \quad \text{for } t \in (0, T],$$

where $\mathfrak{J}^{1-\alpha}$ denotes the Riemann-Liouville fractional integral operator [6]:

$$\mathfrak{J}^{1-\alpha} \mathcal{U}(\cdot, t) = \frac{1}{\Gamma(1-\alpha)} \int_{s=0}^t (t-s)^{-\alpha} \mathcal{U}(\cdot, s) ds, \quad t \in (0, T].$$

Further,

$$\begin{aligned} \mathcal{L}\mathcal{U}(x, t) &:= p(x) \frac{\partial^2 \mathcal{U}}{\partial x^2} - q(x) \frac{\partial \mathcal{U}}{\partial x} - r(x) \mathcal{U}(x, t), \\ \mathfrak{L}\mathcal{U}(x, y, t) &:= p_1(x, y) \frac{\partial^2 \mathcal{U}}{\partial x^2} + p_2(x, y) \frac{\partial^2 \mathcal{U}}{\partial y^2} - q_1(x, y) \frac{\partial \mathcal{U}}{\partial x} - q_2(x, y) \frac{\partial \mathcal{U}}{\partial y} - r_1(x, y) \mathcal{U}(x, y, t). \end{aligned}$$

Again, $p, q, r, f, g, h_1, h_2, h_3, h_4, p_1, p_2, q_1, q_2$ are sufficiently smooth functions with $r(x) \geq r_0 \geq 0$, $p(x) \geq p_0 > 0 \forall x \in [0, L]$ and $r_1(x, y) \geq \tilde{r}_0 \geq 0$, $p_1(x, y) \geq \tilde{p}_0 > 0$, $p_2(x, y) \geq \hat{p}_0 > 0 \forall (x, y) \in \mathcal{G}$. Further, $q, q_1, q_2 \geq 0$. The kernel \mathcal{K} is also smooth and is considered to be positive real-valued. μ is a fixed positive constant.

In the literature, several attempts have been made to develop accurate, stable, and high-order approximations for fractional derivatives. Among them, the $L1$ discretization is a good approximation, which has been used widely in [21, 22], for the fractional problems having initial weak singularities. The method gives a first order convergence on any subdomain away from the origin whereas, it produces less rate of convergence over the entire region (for example have a look at [8, 23]). Even though the nonuniform mesh is more effective than the uniform mesh to capture the initial layer, it fails to occur with second-order accuracy [24]. Further, considering the higher regularity assumption to the solution of the fractional problems, the $L1$ discretization gives $O((\Delta t)^{2-\alpha})$ accuracy [25], where Δt denotes the step length towards time direction. In an attempt to develop a high-order accuracy, Gao *et al.* [26] developed an efficient approximation called $L1-2$ scheme, that gives $O((\Delta t)^{3-\alpha})$ temporal accuracy at t_n ($n \geq 2$) but at t_1 , it produces $O((\Delta t)^{2-\alpha})$ convergence rate. On the other hand, Alikhanov [27] constructed $L2-1_\sigma$ scheme which generates a temporal accuracy $O((\Delta t)^{3-\alpha})$ for all t_n ($n \geq 1$).

In the present work, the $L2-1_\sigma$ scheme is proposed to discretize the time-fractional operator in order to obtain a higher-order temporal accuracy. For the one-dimensional integro-PDEs (1.1), second-order finite difference approximations are used to discretize the spatial derivatives, and a repeated quadrature rule based on trapezoidal approximation is employed to discretize the Volterra operator. The two-dimensional integro-PDEs (1.2) are approximated by making the model in a semi-discretized form by utilizing $L2-1_\sigma$ scheme and composite trapezoidal rule. Then the spatial derivatives are approximated by two-dimensional Haar wavelets. The collocation method is used to solve the linear system. The error analysis is carried out for both models which shows that the methods give a second-order accuracy. The numerical examples confirm the theoretical arguments. In addition, we compare our results with the results obtained by the $L1$ scheme through several graphs and tables. It is proved that the present methods not only give higher-order accuracy but also produce less error compared to the $L1$ scheme.

1.1. A physical motivation

Consider the problem

$$\begin{cases} \partial_t^\alpha \mathcal{U}(x, t) - p(x) \frac{\partial^2 \mathcal{U}}{\partial x^2}(x, t) = f(x, t), & (x, t) \in \Omega, \\ \mathcal{U}(x, 0) = g(x) \quad \forall x \in [0, L], \\ \mathcal{U}(0, t) = h_1(t) \text{ and } \mathcal{U}(1, t) = h_2(t) \quad \forall t \in (0, T]. \end{cases} \quad (1.3)$$

The model (1.3) represents a nonhomogeneous fractional order sub-diffusion model that describes the well-known fractional time random walk [28], which can be obtained from (1.1) by taking $q = r = \mu = 0$. Thus, the model described in (1.1) is a more general case of (1.3). For a more practical implementation of the above problem, the reader can refer to the book [29] and the articles [30, 31].

Such phenomena can also be occurred in the field of viscoelastic dynamical systems, where the coefficient $p(x)$ demonstrates the Newtonian contribution in the viscosity and the integral term is occurred due to viscoelasticity. To illustrate this, let us consider the generalized version of the fractional order viscoelastic model [5, 32]

$$\sigma(x, t) + \varrho_\epsilon^\alpha \partial_t^\alpha \sigma(x, t) = E_0 \left(\epsilon(x, t) + \varrho_\sigma^\beta \partial_t^\beta \epsilon(x, t) \right), \quad \alpha < \beta, \quad (1.4)$$

where σ, ϵ denote the stress and strain, respectively. E_0 is the prolonged modulus of the elasticity. ϱ_ϵ and ϱ_σ represent the relaxation and retardation times, respectively. Further, α, β are the order of the fractional operators that lie between 0 and 1. The model (1.4) represents instantaneous elasticity and describes wave processes since $\alpha < \beta$ whereas, for $\alpha = \beta$, it lacks instantaneous elasticity and

describes diffusion processes. Now, applying \mathfrak{J}^α on the both sides of (1.4) to get

$$\partial_t^\gamma \epsilon(x, t) + \frac{1}{\varrho_\sigma^\beta \Gamma(\alpha)} \int_0^t (t-s)^{\alpha-1} \epsilon(x, s) ds = \mathcal{F}(x, t), \quad (1.5)$$

where $\gamma = \beta - \alpha \in (0, 1)$, and $\mathcal{F}(x, t) = \frac{\varrho_\epsilon^\alpha}{E_0 \varrho_\sigma^\beta} \sigma(x, t) + \frac{1}{E_0 \varrho_\sigma^\beta \Gamma(\alpha)} \int_0^t (t-s)^{\alpha-1} \sigma(x, s) ds$. Here, the stress σ is considered to be known with $\sigma(x, 0) = 0$, and the strain function ϵ is unknown that satisfies the initial condition $\epsilon(x, 0) = 0$. Notice that (1.5) can be obtained by setting $p = q = r = 0$ in the model (1.1). Thus, the present problems described in (1.1) and (1.2) are more general version of (1.3) and (1.5).

Notation: Throughout the paper, we denote C as a generic positive constant independent of the mesh parameter which can take different values at different places. Further, $C_{x,t}^{4,3}(\bar{\Omega}, \mathbb{R})$ represents the space of all real-valued functions whose fourth and third derivatives with respect to x and t , respectively, exist and are continuous. Then, for any $\mathcal{V} \in C_{x,t}^{4,3}(\bar{\Omega}, \mathbb{R})$, we define

$$\|\mathcal{V}\|_{C_{x,t}^{4,3}(\bar{\Omega})} := \|\mathcal{V}\|_\infty + \sum_{j=1}^3 \left\| \frac{\partial^j \mathcal{V}}{\partial t^j} \right\|_\infty + \sum_{j=1}^4 \left\| \frac{\partial^j \mathcal{V}}{\partial x^j} \right\|_\infty,$$

where, $\|\cdot\|_\infty$ denotes the usual sup-norm defined by: $\|\mathcal{V}\|_\infty := \sup_{(x,t) \in \bar{\Omega}} |\mathcal{V}|$.

2. The materialization of analytical quality

Notice that the linear operator $\mathcal{T} \equiv \frac{d^2}{dx^2}$ is not bounded on $C(\bar{\Omega})$ even the the function \mathcal{U} is in $C^3(\bar{\Omega})$. For instance, if we take $\mathcal{U}_n = x^n$, $x \in (0, 1)$ which is bounded on $[0, 1]$ but $\mathcal{T}\mathcal{U}_n = n(n-1)x^{n-2}$ is blowing up as $n \rightarrow \infty$. For this reason, the usual Banach fixed point theorem will not guarantee the existence of a unique solution of the given models (1.1) and (1.2). We need to take special care in order to show its existence and uniqueness. Apply \mathfrak{J}^α on the both sides of (1.1) to get

$$\begin{aligned} \mathcal{U}(x, t) = & g(x) + p(x) \mathfrak{J}^\alpha \left[\frac{\partial^2 \mathcal{U}}{\partial x^2} \right] - q(x) \mathfrak{J}^\alpha \left[\frac{\partial \mathcal{U}}{\partial x} \right] - r(x) \mathfrak{J}^\alpha [\mathcal{U}(x, t)] - \mathfrak{J}^\alpha \left[\mu \int_0^t \mathcal{K}(x, t - \xi) \mathcal{U}(x, \xi) d\xi \right] \\ & + \mathfrak{J}^\alpha [f(x, t)]. \end{aligned} \quad (2.1)$$

Theorem 2.1. *Given that the functions p, q, r, f, g and the kernel \mathcal{K} are sufficiently smooth with $p_{xx} \leq 0$, $q_x \leq 0$, the existence of a unique solution $\mathcal{U} \in C_{x,t}^{4,3}(\bar{\Omega}, \mathbb{R})$ to the given problem (1.1) can be guaranteed.*

Proof. Define an operator $\mathbf{F} : C_{x,t}^{4,3}(\bar{\Omega}, \mathbb{R}) \rightarrow C_{x,t}^{4,3}(\bar{\Omega}, \mathbb{R})$ such that

$$\begin{aligned} \mathbf{F}\mathcal{U}(x, t) = & g(x) + p(x) \mathfrak{J}^\alpha \left[\frac{\partial^2 \mathcal{U}}{\partial x^2} \right] - q(x) \mathfrak{J}^\alpha \left[\frac{\partial \mathcal{U}}{\partial x} \right] - r(x) \mathfrak{J}^\alpha [\mathcal{U}(x, t)] - \mathfrak{J}^\alpha \left[\mu \int_0^t \mathcal{K}(x, t - \xi) \mathcal{U}(x, \xi) d\xi \right] \\ & + \mathfrak{J}^\alpha [f(x, t)]. \end{aligned}$$

Then, from (2.1), we have $\mathcal{U}(x, t) = \mathbf{F}\mathcal{U}(x, t)$, for $(x, t) \in \bar{\Omega}$. In order to show \mathbf{F} to be compact, we need to prove $\{\mathbf{F}u_n\}$ is bounded, and equicontinuous [33] on $C_{x,t}^{4,3}(\bar{\Omega}, \mathbb{R})$ for any bounded sequence $\{u_n\}$ in $C_{x,t}^{4,3}(\bar{\Omega}, \mathbb{R})$. Then, the Arzela-Ascoli's theorem [34] confirms the existence of a uniformly convergent subsequence of $\{\mathbf{F}u_n\}$ with respect to the norm $\|\cdot\|_\infty$.

Let us take $\|\cdot\|_\infty$ on both sides of the above equation and then, apply triangle inequality to have

$$\begin{aligned} \|\mathbf{F}\mathcal{U}_n\|_\infty &\leq \|g\|_\infty + \|p\|_\infty \mathfrak{J}^\alpha \left[\left\| \frac{\partial^2 \mathcal{U}_n}{\partial x^2} \right\|_\infty \right] + \|q\|_\infty \mathfrak{J}^\alpha \left[\left\| \frac{\partial \mathcal{U}_n}{\partial x} \right\|_\infty \right] + \|r\|_\infty \mathfrak{J}^\alpha [\|\mathcal{U}_n\|_\infty] \\ &\quad + \mathfrak{J}^\alpha \left[\mu \int_0^t \|\mathcal{K}\|_\infty \|\mathcal{U}_n\|_\infty d\xi \right] + \mathfrak{J}^\alpha [\|f(x, t)\|_\infty] \\ &\leq \|g\|_\infty + \frac{T^\alpha [(\alpha + 1)(\|p\|_\infty + \|q\|_\infty + \|r\|_\infty) + T\mu\|\mathcal{K}\|_\infty]}{\Gamma(\alpha + 2)} \|\mathcal{U}_n\|_{C_{x,t}^{4,3}(\bar{\Omega})} + \frac{\|f\|_\infty T^\alpha}{\Gamma(\alpha + 1)}. \end{aligned}$$

Notice that the functions p, q, r, g, f and the kernel \mathcal{K} are sufficiently smooth function, and $\{\mathcal{U}_n\}$ is bounded in $C_{x,t}^{4,3}(\bar{\Omega}, \mathbb{R})$. Hence, there exists a real number $\mathfrak{M}_1 > 0$ such that $\|\mathbf{F}\mathcal{U}_n\|_\infty \leq \mathfrak{M}_1$ for all $n \in \mathbb{N}$, $(x, t) \in \bar{\Omega}$. This proves that $\{\mathbf{F}\mathcal{U}_n\}$ is bounded. Further, let $\epsilon > 0$ be given. For any $\mathcal{U}_n \in C_{x,t}^{4,3}(\bar{\Omega}, \mathbb{R})$, consider

$$\begin{aligned} \left| \mathbf{F}\mathcal{U}_n(x, t) - \mathbf{F}\mathcal{U}_n(y, t) \right| &\leq |g(x) - g(y)| + |p(x)| \mathfrak{J}^\alpha \left[\left| \frac{\partial^2 \mathcal{U}_n}{\partial x^2}(x, t) - \frac{\partial^2 \mathcal{U}_n}{\partial x^2}(y, t) \right| \right] \\ &\quad + |p(x) - p(y)| \mathfrak{J}^\alpha \left[\left| \frac{\partial^2 \mathcal{U}_n}{\partial x^2}(y, t) \right| \right] + |q(x)| \mathfrak{J}^\alpha \left[\left| \frac{\partial \mathcal{U}_n}{\partial x}(x, t) - \frac{\partial \mathcal{U}_n}{\partial x}(y, t) \right| \right] \\ &\quad + |q(x) - q(y)| \mathfrak{J}^\alpha \left[\left| \frac{\partial \mathcal{U}_n}{\partial x}(y, t) \right| \right] + |r(x)| \mathfrak{J}^\alpha [|\mathcal{U}_n(x, t) - \mathcal{U}_n(y, t)|] \\ &\quad + |r(x) - r(y)| \mathfrak{J}^\alpha [|\mathcal{U}_n(y, t)|] + \mathfrak{J}^\alpha \left[\mu \int_0^t \left(|\mathcal{K}| |\mathcal{U}_n(x, \xi) - \mathcal{U}_n(y, \xi)| \right. \right. \\ &\quad \left. \left. + |\mathcal{K}(x, t - \xi) - \mathcal{K}(y, t - \xi)| |\mathcal{U}_n(y, \xi)| \right) d\xi \right] + \mathfrak{J}^\alpha [|f(x, t) - f(y, t)|]. \end{aligned}$$

Lagrange's Mean Value theorem yields the following

$$\begin{aligned} \left| \mathbf{F}\mathcal{U}_n(x, t) - \mathbf{F}\mathcal{U}_n(y, t) \right| &\leq |x - y| |g'(\theta_1)| + \frac{|x - y| T^\alpha}{\Gamma(\alpha + 1)} \left(|p(x)| \left| \frac{\partial^3 \mathcal{U}_n}{\partial x^3}(\theta_2, t) \right| + |p'(\theta_3)| \left| \frac{\partial^2 \mathcal{U}_n}{\partial x^2}(y, t) \right| \right) \\ &\quad + \frac{|x - y| T^\alpha}{\Gamma(\alpha + 1)} \left(|q(x)| \left| \frac{\partial^2 \mathcal{U}_n}{\partial x^2}(\theta_4, t) \right| + |q'(\theta_5)| \left| \frac{\partial \mathcal{U}_n}{\partial x}(y, t) \right| \right) \\ &\quad + \frac{|x - y| T^\alpha}{\Gamma(\alpha + 1)} \left(|r(x)| \left| \frac{\partial \mathcal{U}_n}{\partial x}(\theta_6, t) \right| + |r'(\theta_7)| |\mathcal{U}_n(y, t)| \right) \\ &\quad + \frac{|x - y| \mu T^{\alpha+1}}{\Gamma(\alpha + 2)} \left(|\mathcal{K}| \left| \frac{\partial \mathcal{U}_n}{\partial x}(\theta_8, \xi) \right| + \left| \frac{\partial \mathcal{K}}{\partial x}(\theta_9, t - \xi) \right| |\mathcal{U}_n(y, \xi)| \right) \\ &\quad + \frac{|x - y| T^\alpha}{\Gamma(\alpha + 1)} \left| \frac{\partial f}{\partial x}(\theta_{10}, t) \right|, \end{aligned}$$

where $x < \theta_i < y$ for $i = 1, 2, \dots, 10$. Notice that, $p, q, r, f, g, \mathcal{K}$ are sufficiently smooth, and $\mathcal{U}_n \in C_{x,t}^{4,3}(\bar{\Omega}, \mathbb{R})$. Hence we have

$$\left| \mathbf{F}\mathcal{U}_n(x, t) - \mathbf{F}\mathcal{U}_n(y, t) \right| \leq |x - y| \mathfrak{M}_2,$$

where \mathfrak{M}_2 is the upper bound of the right-hand side expression sans the factor $|x - y|$. Let us choose $\delta = \min \left\{ \epsilon, \frac{\epsilon}{\mathfrak{M}_2} \right\}$, and take $|x - y| < \delta$ to yield

$$\left| \mathbf{F}\mathcal{U}_n(x, t) - \mathbf{F}\mathcal{U}_n(y, t) \right| < \epsilon, \quad \text{for all } n \in \mathbb{N}, t \in (0, T].$$

Hence, $\{\mathbf{F}\mathcal{U}_n\}$ is equicontinuous. Therefore, by the Arzela-Ascoli's theorem, $\{\mathbf{F}\mathcal{U}_n\}$ has a subsequence that converges uniformly and hence converges with respect to the norm $\|\cdot\|_\infty$. Then, the Schauder fixed point theorem [35] confirms the existence of a solution $\mathcal{U} \in C_{x,t}^{4,3}(\bar{\Omega}, \mathbb{R})$ for (1.1).

In order to prove the unicity, let $\mathcal{U}_1, \mathcal{U}_2$ be two solutions of (1.1), Then $\mathcal{W} = \mathcal{U}_1 - \mathcal{U}_2$ will be a solution of

$$\begin{cases} \partial_t^\alpha \mathcal{W}(x, t) - \mathcal{L}\mathcal{W}(x, t) + \mu \int_0^t \mathcal{K}(x, t - \xi) \mathcal{W}(x, \xi) d\xi = 0, & (x, t) \in \Omega, \\ \mathcal{W}(x, 0) = 0 & \text{for } x \in [0, L], \\ \mathcal{W}(0, t) = \mathcal{W}(1, t) = 0 & \text{for } t \in (0, T]. \end{cases}$$

Our aim is to show that \mathcal{W} is identically zero. Let us take $\mathcal{W} = \mathcal{W}^+ - \mathcal{W}^-$, with $\mathcal{W}^+ := \max\{0, \mathcal{W}\}$ and $\mathcal{W}^- := \max\{0, -\mathcal{W}\}$.

$$\begin{aligned} \int_0^L \partial_t^\alpha (\mathcal{W}^+ - \mathcal{W}^-) \mathcal{W}^+ dx &= \int_0^L p(\mathcal{W}_{xx}^+ - \mathcal{W}_{xx}^-) \mathcal{W}^+ dx - \int_0^L q(\mathcal{W}_x^+ - \mathcal{W}_x^-) \mathcal{W}^+ dx \\ &\quad - \int_0^L r(\mathcal{W}^+ - \mathcal{W}^-) \mathcal{W}^+ dx - \int_0^L \left(\mu \int_0^t \mathcal{K}(\mathcal{W}^+ - \mathcal{W}^-) d\xi \right) \mathcal{W}^+ dx. \end{aligned}$$

Integrating by parts and a simple calculation gives

$$\begin{aligned} \int_0^L \left(\partial_t^\alpha \mathcal{W}^+ \right) \mathcal{W}^+ dx &= \frac{1}{2} \int_0^L p_{xx} (\mathcal{W}^+)^2 dx - \int_0^L p (\mathcal{W}_x^+)^2 dx + \frac{1}{2} \int_0^L q_x (\mathcal{W}^+)^2 dx \\ &\quad - \int_0^L r (\mathcal{W}^+)^2 dx - \int_0^L \left(\mu \int_0^t \mathcal{K} \mathcal{W}^+ d\xi \right) \mathcal{W}^+ dx. \end{aligned}$$

Notice that $\mathcal{W}^+ \geq 0$. Under the assumption that $p_{xx} \leq 0$, $q_x \leq 0$, the right-hand side of the above expression is ≤ 0 . This yields $\partial_t^\alpha \mathcal{W}^+ \leq 0$, which implies $\mathcal{W}_t^+ \leq 0$. Then \mathcal{W}^+ decreases as t increases with $\mathcal{W}^+(x, 0) = 0$. This is possible only when $\mathcal{W}^+ = 0$. In a similar way, it can be proved that $\mathcal{W}^- = 0$. Therefore $\mathcal{W} \equiv 0$ and hence $\mathcal{U}_1 \equiv \mathcal{U}_2$. \square

Theorem 2.2. *Given that the functions $p_1, p_2, q_1, q_2, r_1, f, g$ and the kernel \mathcal{K} are sufficiently smooth with $(p_1)_{xx}, (p_2)_{xx} \leq 0$, $(q_1)_x, (q_2)_x \leq 0$, the existence of a unique solution $\mathcal{U} \in C_{\mathbf{x},t}^{4,3}(\bar{\mathcal{G}} \times [0, T], \mathbb{R})$ to the given problem (1.2) can be guaranteed. $\mathbf{x} := (x, y) \in \mathcal{G}$ and $C_{\mathbf{x},t}^{4,3}(\bar{\mathcal{G}} \times [0, T], \mathbb{R})$ denotes the space of all real-valued functions, whose fourth derivatives with respect to x, y including mixed derivatives, and third derivative with respect to t , exist and continuous.*

Proof. This theorem can be proved in a similar way as described in Theorem 2.1 \square

3. Numerical methods

This section comprises the procedure of the construction of the numerical schemes to solve the one and two-dimensional fractional integro-PDEs depicted in (1.1) and (1.2).

3.1. Approximation of one-dimensional integro-PDEs

To solve the One-dimensional integro-PDEs (1.1), we approximate the Caputo derivative by $L2-1_\sigma$ scheme, the spatial derivatives are discretized by central difference operators, and the composite trapezoidal formula is used to deal with the Volterra integral operator. Let $M, N \in \mathbb{N}$ be fixed. Set: $\Delta x = L/M, \Delta t = T/N$. The mesh points are defined as $x_m = m\Delta x, t_n = n\Delta t, m = 0, 1, \dots, M; n = 0, 1, \dots, N$. Thus, the discrete domain is given by: $\Omega_{M,N} := \{(x_m, t_n) : m = 0, 1, \dots, M; n = 0, 1, \dots, N\}$. Suppose $\{\mathcal{U}_m^n\}_{m=0, n=0}^{M,N}$ denote the mesh function approximating $\mathcal{U}(x, t)$ at each (x_m, t_n) . Further, we denote $t_{n+\sigma} = t_n + \sigma\Delta t$ for some constant $\sigma \in (0, 1)$. At the mesh point $(x_m, t_{n+\sigma})$, the

fractional Caputo derivative is redefined as:

$$\begin{aligned}\partial_t^\alpha \mathcal{U}(x_m, t_{n+\sigma}) &= \frac{1}{\Gamma(1-\alpha)} \int_{t_0}^{t_{n+\sigma}} (t_{n+\sigma} - \rho)^{-\alpha} \frac{\partial \mathcal{U}}{\partial \rho}(x_m, \rho) d\rho \\ &= \frac{1}{\Gamma(1-\alpha)} \left(\sum_{j=1}^n \int_{t_{j-1}}^{t_j} (t_{n+\sigma} - \rho)^{-\alpha} \frac{\partial \mathcal{U}}{\partial \rho}(x_m, \rho) d\rho + \int_{t_n}^{t_{n+\sigma}} (t_{n+\sigma} - \rho)^{-\alpha} \frac{\partial \mathcal{U}}{\partial \rho}(x_m, \rho) d\rho \right)\end{aligned}\quad (3.1)$$

The basic idea of $L2-1_\sigma$ formula is that the function $\mathcal{U}(x_m, t)$ is approximated by a quadratic interpolation $\mathcal{P}_{2,n}(x_m, t)$ over the interval (t_{n-1}, t_n) , $n = 1, 2, \dots, N-1$ and in the interval (t_n, t_{n+1}) , $n = 0, 1, \dots, N-1$, it is approximated by a linear interpolation $\mathcal{P}_{1,n}(x_m, t)$. The interpolations are defined as:

$$\begin{cases} \mathcal{P}_{2,n}(x_m, t) = \frac{(t-t_n)(t-t_{n+1})}{2(\Delta t)^2} \mathcal{U}_m^{n-1} - \frac{(t-t_{n-1})(t-t_{n+1})}{(\Delta t)^2} \mathcal{U}_m^n + \frac{(t-t_{n-1})(t-t_n)}{2(\Delta t)^2} \mathcal{U}_m^{n+1}, \\ \mathcal{P}_{1,n}(x_m, t) = \frac{t_{n+1}-t}{\Delta t} \mathcal{U}_m^n + \frac{t-t_n}{\Delta t} \mathcal{U}_m^{n+1}. \end{cases}$$

Differentiating with respect to t we have

$$\begin{cases} \mathcal{P}'_{2,n}(x_m, t) = \left(\frac{t_{n+\frac{1}{2}}-t}{\Delta t} \right) \left(\frac{\mathcal{U}_m^n - \mathcal{U}_m^{n-1}}{\Delta t} \right) + \left(\frac{t-t_{n-\frac{1}{2}}}{\Delta t} \right) \left(\frac{\mathcal{U}_m^{n+1} - \mathcal{U}_m^n}{\Delta t} \right), \\ \mathcal{P}'_{1,n}(x_m, t) = \frac{\mathcal{U}_m^{n+1} - \mathcal{U}_m^n}{\Delta t}. \end{cases}$$

Hence, we have the following discretization for fractional Caputo derivative:

$$\begin{aligned}\partial_t^\alpha \mathcal{U}(x_m, t_{n+\sigma}) &\approx {}^{L2-1_\sigma} \mathcal{D}_N^\alpha \mathcal{U}_m^{n+\sigma} := \frac{1}{\Gamma(1-\alpha)} \left(\sum_{j=1}^n \int_{t_{j-1}}^{t_j} (t_{n+\sigma} - \rho)^{-\alpha} \mathcal{P}'_{2,n}(x_m, \rho) d\rho \right. \\ &\quad \left. + \int_{t_n}^{t_{n+\sigma}} (t_{n+\sigma} - \rho)^{-\alpha} \mathcal{P}'_{1,n}(x_m, \rho) d\rho \right) \\ &= \sum_{j=0}^n d_j^{n+1} (\mathcal{U}_m^{j+1} - \mathcal{U}_m^j).\end{aligned}\quad (3.2)$$

Here, $d_0^1 = \frac{a_0}{(\Delta t)^\alpha \Gamma(2-\alpha)}$, and for $n \geq 1$

$$d_j^{n+1} = \frac{1}{(\Delta t)^\alpha \Gamma(2-\alpha)} \begin{cases} a_n - b_n, & j = 0, \\ b_{n-j+1} + a_{n-j} - b_{n-j}, & 1 \leq j \leq n-1, \\ a_0 + b_1, & j = n, \end{cases}\quad (3.3)$$

with $a_0 = \sigma^{1-\alpha}$, $a_k = (k+\sigma)^{1-\alpha} - (k-1+\sigma)^{1-\alpha}$, $k \geq 1$, and $b_k = \frac{1}{2-\alpha} [(k+\sigma)^{2-\alpha} - (k-1+\sigma)^{2-\alpha}] - \frac{1}{2} [(k+\sigma)^{1-\alpha} + (k-1+\sigma)^{1-\alpha}]$, $k \geq 1$. The algorithm for the computation of d_j^{n+1} is given in Algorithm 1.

The following lemma helps to discretize the spatial derivatives as well as to estimate the truncation error bound for the proposed schemes.

Algorithm 1 COMPUTATION OF d_j^{n+1}

```

1: Input 1:  $\alpha$  ▷ Order of the fractional operator
2: Input 2:  $M$  ▷ Number of mesh interval towards space
3: Input 3:  $N$  ▷ Number of mesh interval towards time
4: Compute  $\sigma = 1 - (\alpha/2)$ 
5: Compute  $\Delta t = T/N$ 
6: Compute  $a_0 = \sigma^{1-\alpha}$ 
7: for  $k = 1, 2, \dots, N$  do
8:    $a_k = (k + \sigma)^{1-\alpha} - (k - 1 + \sigma)^{1-\alpha}$ 
9:    $b_k = ((k + \sigma)^{2-\alpha} - (k - 1 + \sigma)^{2-\alpha})/(2 - \alpha) - ((k + \sigma)^{1-\alpha} + (k - 1 + \sigma)^{1-\alpha})/2$ 
10: end for
11: Compute  $d_0^1 = a_0/((\Delta t)^\alpha \Gamma(2 - \alpha))$ 
12: for  $n = 1, 2, \dots, N - 1$  do
13:   for  $j = 0, 1, \dots, n - 1$  do
14:     if  $j = 0$  then
15:        $d_j^{n+1} = (a_n - b_n)/((\Delta t)^\alpha \Gamma(2 - \alpha))$ 
16:     else if  $j = n$  then
17:        $d_j^{n+1} = (a_0 + b_1)/((\Delta t)^\alpha \Gamma(2 - \alpha))$ 
18:     else
19:        $d_j^{n+1} = (b_{n-j+1} + a_{n-j} - b_{n-j})/((\Delta t)^\alpha \Gamma(2 - \alpha))$ 
20:     end if
21:   end for
22: end for
23: Output: Return of  $d_j^{n+1}$ 

```

Lemma 3.1. For any $\phi(t) \in C^2([0, T])$, and $n = 0, 1, \dots, N - 1$, we have

$$\phi(t_{n+\sigma}) = \sigma\phi(t_{n+1}) + (1 - \sigma)\phi(t_n) + O((\Delta t)^2), \quad \sigma \in (0, 1).$$

Proof. Using the Taylor series expansion, one can easily verify the result. □

Therefore, $\frac{\partial^2 \mathcal{U}}{\partial x^2}$ and $\frac{\partial \mathcal{U}}{\partial x}$ can be approximated as:

$$\begin{aligned} \frac{\partial^2 \mathcal{U}}{\partial x^2}(x_m, t_{n+\sigma}) &= \sigma \frac{\partial^2 \mathcal{U}}{\partial x^2}(x_m, t_{n+1}) + (1 - \sigma) \frac{\partial^2 \mathcal{U}}{\partial x^2}(x_m, t_n) + O((\Delta t)^2) \\ &\approx \frac{\sigma}{(\Delta x)^2} (\mathcal{U}_{m-1}^{n+1} - 2\mathcal{U}_m^{n+1} + \mathcal{U}_{m+1}^{n+1}) + \frac{1 - \sigma}{(\Delta x)^2} (\mathcal{U}_{m-1}^n - 2\mathcal{U}_m^n + \mathcal{U}_{m+1}^n) + O((\Delta t)^2 + (\Delta x)^2) \\ &= \delta_{\Delta x, \Delta t}^2 \mathcal{U}_m^{n+\sigma} + O((\Delta t)^2 + (\Delta x)^2), \end{aligned} \tag{3.4}$$

provided $\mathcal{U} \in C_{x,t}^{4,3}(\bar{\Omega}, \mathbb{R})$, where $\delta_{\Delta x, \Delta t}^2 \mathcal{U}_m^{n+\sigma} = \frac{\sigma}{h^2} (\mathcal{U}_{m-1}^{n+1} - 2\mathcal{U}_m^{n+1} + \mathcal{U}_{m+1}^{n+1}) + \frac{1 - \sigma}{h^2} (\mathcal{U}_{m-1}^n - 2\mathcal{U}_m^n + \mathcal{U}_{m+1}^n)$, and

$$\begin{aligned} \frac{\partial \mathcal{U}}{\partial x}(x_m, t_{n+\sigma}) &= \sigma \frac{\partial \mathcal{U}}{\partial x}(x_m, t_{n+1}) + (1 - \sigma) \frac{\partial \mathcal{U}}{\partial x}(x_m, t_n) + O((\Delta t)^2) \\ &\approx \frac{\sigma}{2\Delta x} (\mathcal{U}_{m+1}^{n+1} - \mathcal{U}_{m-1}^{n+1}) + \frac{1 - \sigma}{2\Delta x} (\mathcal{U}_{m+1}^n - \mathcal{U}_{m-1}^n) + O((\Delta t)^2 + (\Delta x)^2) \\ &= D_{\Delta x, \Delta t}^0 \mathcal{U}_m^{n+\sigma} + O((\Delta t)^2 + (\Delta x)^2), \end{aligned} \tag{3.5}$$

where $D_{\Delta x, \Delta t}^0 \mathcal{U}_m^{n+\sigma} = \frac{\sigma}{2\Delta x} (\mathcal{U}_{m+1}^{n+1} - \mathcal{U}_{m-1}^{n+1}) + \frac{1 - \sigma}{2\Delta x} (\mathcal{U}_{m+1}^n - \mathcal{U}_{m-1}^n)$. Now, it remains to discretize

the Volterra integral operator which is given as:

$$\begin{aligned}
\int_0^{t_{n+\sigma}} \mathcal{K}(x_m, t_{n+\sigma} - \xi) \mathcal{U}(x_m, \xi) d\xi &= \sum_{j=0}^{n-1} \int_{t_j}^{t_{j+1}} \mathcal{K}(x_m, t_{n+\sigma} - \xi) \mathcal{U}(x_m, \xi) d\xi \\
&\quad + \int_{t_n}^{t_{n+\sigma}} \mathcal{K}(x_m, t_{n+\sigma} - \xi) \mathcal{U}(x_m, \xi) d\xi \\
&= \frac{\Delta t}{2} \sum_{j=0}^{n-1} [\mathcal{K}(x_m, t_{n+\sigma} - t_{j+1}) \mathcal{U}(x_m, t_{j+1}) + \mathcal{K}(x_m, t_{n+\sigma} - t_j) \mathcal{U}(x_m, t_j)] \\
&\quad + \frac{\sigma \Delta t}{2} [\mathcal{K}(x_m, t_{n+\sigma} - t_n) \mathcal{U}(x_m, t_n) + \mathcal{K}(x_m, 0) \mathcal{U}(x_m, t_{n+\sigma})] + O((\Delta t)^2) \\
&\approx \frac{\Delta t}{2} \sum_{j=0}^{n-1} [\mathcal{K}(x_m, t_{n+\sigma} - t_{j+1}) \mathcal{U}_m^{j+1} + \mathcal{K}(x_m, t_{n+\sigma} - t_j) \mathcal{U}_m^j] + \frac{\sigma \Delta t}{2} \mathcal{K}(x_m, t_{n+\sigma} - t_n) \mathcal{U}_m^n \\
&\quad + \frac{\sigma \Delta t}{2} \mathcal{K}(x_m, 0) [\sigma \mathcal{U}_m^{n+1} + (1 - \sigma) \mathcal{U}_m^n] + O((\Delta t)^2) \\
&= \mathcal{I}_N \mathcal{U}_m^{n+\sigma} + O((\Delta t)^2), \tag{3.6}
\end{aligned}$$

where $\mathcal{I}_N \mathcal{U}_m^{n+\sigma} = \frac{\Delta t}{2} \sum_{j=0}^{n-1} [\mathcal{K}(x_m, t_{n+\sigma} - t_{j+1}) \mathcal{U}_m^{j+1} + \mathcal{K}(x_m, t_{n+\sigma} - t_j) \mathcal{U}_m^j] + \frac{\sigma \Delta t}{2} \mathcal{K}(x_m, t_{n+\sigma} - t_n) \mathcal{U}_m^n + \frac{\sigma \Delta t}{2} \mathcal{K}(x_m, 0) [\sigma \mathcal{U}_m^{n+1} + (1 - \sigma) \mathcal{U}_m^n]$. Based on the above discretizations discussed in (3.2)–(3.6), we have

$$\left\{ \begin{array}{l}
L^{2-1_\sigma} \mathcal{D}_N^\alpha \mathcal{U}(x_m, t_{n+\sigma}) - p(x_m) \delta_{\Delta x, \Delta t}^2 \mathcal{U}(x_m, t_{n+\sigma}) + q(x_m) D_{\Delta x, \Delta t}^0 \mathcal{U}(x_m, t_{n+\sigma}) \\
\quad + r(x_m) \mathcal{U}(x_m, t_{n+\sigma}) + \mu \mathcal{I}_N \mathcal{U}(x_m, t_{n+\sigma}) = f(x_m, t_{n+\sigma}) + L^{2-1_\sigma} \mathcal{R}_m^{n+\sigma}, \\
\text{for } m = 1, 2, \dots, M-1; n = 0, 1, \dots, N-1, \\
\mathcal{U}(x_m, t_0) = g(x_m) \text{ for } m = 0, 1, \dots, M, \\
\mathcal{U}(x_0, t_n) = h_1(t_n) \text{ and } \mathcal{U}(x_M, t_n) = h_2(t_n) \text{ for } n = 0, 1, \dots, N.
\end{array} \right. \tag{3.7}$$

$L^{2-1_\sigma} \mathcal{R}_m^{n+\sigma}$ is the remainder term given by

$$L^{2-1_\sigma} \mathcal{R}_m^{n+\sigma} = \left(\partial_t^\alpha - L^{2-1_\sigma} \mathcal{D}_N^\alpha \right) \mathcal{U}(x_m, t_{n+\sigma}) + O((\Delta t)^2 + (\Delta x)^2). \tag{3.8}$$

Hence, the discrete version of (1.1) can be obtained as:

$$\left\{ \begin{array}{l}
L^{2-1_\sigma} \mathcal{D}_N^\alpha \mathcal{U}_m^{n+\sigma} - p(x_m) \delta_{\Delta x, \Delta t}^2 \mathcal{U}_m^{n+\sigma} + q(x_m) D_{\Delta x, \Delta t}^0 \mathcal{U}_m^{n+\sigma} \\
\quad + r(x_m) \mathcal{U}_m^{n+\sigma} + \mu \mathcal{I}_N \mathcal{U}_m^{n+\sigma} = f(x_m, t_{n+\sigma}), \\
\text{for } m = 1, 2, \dots, M-1; n = 0, 1, \dots, N-1, \\
\mathcal{U}_m^0 = g(x_m) \text{ for } m = 0, 1, \dots, M, \\
\mathcal{U}_0^n = h_1(t_n) \text{ and } \mathcal{U}_M^n = h_2(t_n) \text{ for } n = 0, 1, \dots, N.
\end{array} \right. \tag{3.9}$$

A simple calculation yields the following implicit scheme:

$$\left\{ \begin{array}{l} \mathcal{A}_{m-1}\mathcal{U}_{m-1}^{n+1} + \mathcal{B}_m\mathcal{U}_m^{n+1} + \mathcal{C}_{m+1}\mathcal{U}_{m+1}^{n+1} = \tilde{\mathcal{A}}_{m-1}\mathcal{U}_{m-1}^n + \tilde{\mathcal{B}}_m\mathcal{U}_m^n + \tilde{\mathcal{C}}_{m+1}\mathcal{U}_{m+1}^n + \mathcal{F}_m^n, \\ \text{for } m = 1, 2, \dots, M-1; n = 0, 1, \dots, N-1, \\ \mathcal{U}_m^0 = g(x_m) \text{ for } m = 0, 1, \dots, M, \\ \mathcal{U}_0^n = h_1(t_n) \text{ and } \mathcal{U}_M^n = h_2(t_n) \text{ for } n = 0, 1, \dots, N, \end{array} \right. \quad (3.10)$$

where the coefficients are given by

$$\left\{ \begin{array}{l} \mathcal{A}_{m-1} = -\frac{q(x_m)\sigma}{2\Delta x} - \frac{p(x_m)\sigma}{(\Delta x)^2}, \quad \mathcal{B}_m = d_n^{n+1} + \frac{2p(x_m)\sigma}{(\Delta x)^2} + r(x_m)\sigma + \frac{\mu\sigma^2\Delta t}{2}\mathcal{K}(x_m, 0), \\ \mathcal{C}_{m+1} = \frac{q(x_m)\sigma}{2\Delta x} - \frac{p(x_m)\sigma}{(\Delta x)^2}, \quad \tilde{\mathcal{A}}_{m-1} = \frac{q(x_m)(1-\sigma)}{2\Delta x} + \frac{p(x_m)(1-\sigma)}{(\Delta x)^2}, \\ \tilde{\mathcal{B}}_m = d_n^{n+1} - \frac{2p(x_m)(1-\sigma)}{(\Delta x)^2} - r(x_m)(1-\sigma) - \frac{\mu\Delta t}{2}\mathcal{K}(x_m, t_{n+\sigma} - t_n) \\ \quad - \frac{\mu\sigma\Delta t}{2}\mathcal{K}(x_m, t_{n+\sigma} - t_n) - \frac{\mu\Delta t\sigma(1-\sigma)}{2}\mathcal{K}(x_m, 0), \\ \tilde{\mathcal{C}}_{m+1} = -\frac{q(x_m)(1-\sigma)}{2\Delta x} + \frac{p(x_m)(1-\sigma)}{(\Delta x)^2}, \end{array} \right.$$

for $m = 1, 2, \dots, M-1$; $n = 0, 1, \dots, N-1$. Further, $\mathcal{F}_m^0 = f(x_m, t_\sigma)$, $\mathcal{F}_m^1 = -d_0^2(\mathcal{U}_m^1 - \mathcal{U}_m^0) - \frac{\Delta t}{2}\mathcal{K}(x_m, t_{1+\sigma} - t_0)\mathcal{U}_m^0 + f(x_m, t_{1+\sigma})$, and for $n = 2, 3, \dots, N-1$, we have

$$\begin{aligned} \mathcal{F}_m^n = & -\sum_{j=0}^{n-1} d_j^{n+1}(\mathcal{U}_m^{j+1} - \mathcal{U}_m^j) - \frac{\mu\Delta t}{2}\mathcal{K}(x_m, t_{n+\sigma} - t_{n-1})\mathcal{U}_m^{n-1} - \frac{\mu\Delta t}{2}\sum_{j=0}^{n-2} \left[\mathcal{K}(x_m, t_{n+\sigma} - t_{j+1})\mathcal{U}_m^{j+1} \right. \\ & \left. + \mathcal{K}(x_m, t_{n+\sigma} - t_j)\mathcal{U}_m^j \right] + f(x_m, t_{n+\sigma}). \end{aligned} \quad (3.11)$$

Notice that, at each time level n for $n = 0, 1, \dots, N-1$, the unknowns $\mathcal{U}_1^{n+1}, \mathcal{U}_2^{n+1}, \dots, \mathcal{U}_{M-1}^{n+1}$ can be solved from the implicit discrete scheme (3.10), which can be written as:

$$\mathbf{H}\mathbf{U}^{n+1} = \tilde{\mathbf{H}}\mathbf{U}^n + \mathcal{F}^n,$$

where $\mathbf{U}^{n+1} = (\mathcal{U}_1^{n+1}, \mathcal{U}_2^{n+1}, \dots, \mathcal{U}_{M-1}^{n+1})^T$, $\mathbf{U}^n = (\mathcal{U}_1^n, \mathcal{U}_2^n, \dots, \mathcal{U}_{M-1}^n)^T$, $\mathcal{F}^n = (\mathcal{F}_1^n, \mathcal{F}_2^n, \dots, \mathcal{F}_{M-1}^n)^T$, and the coefficient matrices $\mathbf{H}, \tilde{\mathbf{H}}$ are defined as:

$$\mathbf{H} = \begin{pmatrix} \mathcal{B}_1 & \mathcal{C}_2 & & & & \\ \mathcal{A}_1 & \mathcal{B}_2 & \mathcal{C}_3 & & & \\ & \ddots & \ddots & \ddots & & \\ & & \mathcal{A}_{M-3} & \mathcal{B}_{M-2} & \mathcal{C}_{M-1} & \\ & & & \mathcal{A}_{M-2} & \mathcal{B}_{M-1} & \end{pmatrix}, \quad \tilde{\mathbf{H}} = \begin{pmatrix} \tilde{\mathcal{B}}_1 & \tilde{\mathcal{C}}_2 & & & & \\ \tilde{\mathcal{A}}_1 & \tilde{\mathcal{B}}_2 & \tilde{\mathcal{C}}_3 & & & \\ & \ddots & \ddots & \ddots & & \\ & & \tilde{\mathcal{A}}_{M-3} & \tilde{\mathcal{B}}_{M-2} & \tilde{\mathcal{C}}_{M-1} & \\ & & & \tilde{\mathcal{A}}_{M-2} & \tilde{\mathcal{B}}_{M-1} & \end{pmatrix}.$$

The invertibility of the coefficient matrix \mathbf{H} can be guaranteed from the positivity assumption on the coefficient function $p(x) \geq p_0 > 0$ and the nonrestrictive assumption on the lower bound of the number of space partitions M , which is

$$\frac{L\|q\|_\infty}{2p_0} < M. \quad (3.12)$$

The following algorithms (Algorithm 2 and Algorithm 3) describe the computational techniques for the coefficient matrices $\mathbf{H}_{(M-1) \times (M-1)}$ and $\tilde{\mathbf{H}}_{(M-1) \times (M-1)}$.

Algorithm 2 COMPUTATION OF $\mathbf{H}_{(M-1) \times (M-1)}$

```

1: Input 1:  $\alpha$  ▷ Order of the fractional operator
2: Input 2:  $M$  ▷ Number of mesh interval towards space
3: Input 3:  $N$  ▷ Number of mesh interval towards time
4: Compute  $\sigma = 1 - (\alpha/2)$ 
5: Compute  $\Delta x = L/M$  and  $\Delta t = T/N$  ▷ Mesh parameters
6: Compute  $x_m = m * \Delta x$  for  $m = 0, 1, \dots, M$ 
7: Compute  $t_n = n * \Delta t$  for  $m = 0, 1, \dots, N$ 
8: Compute  $p$  and  $q$  ▷ coefficient functions
9: Compute  $\mathcal{K}$  ▷ The given kernel
10: Compute  $d_0^1$  and  $d_j^{n+1}$  for  $n = 1, 2, \dots, N - 1, j = 0, 1, \dots, n - 1$  using Algorithm 1
11: for  $n = 1, 2, \dots, N$  do
12:   for  $m = 2, 3, \dots, M$  do
13:      $\mathbf{H}_{m-1, m-1} = d_n^{n+1} + (2 * p(x_m) * \sigma / (\Delta x)^2) + \sigma * q(x_m) + (\mu * \sigma^2 * \Delta t * \mathcal{K}(x_m, 0) / 2)$ 
14:   end for
15:   for  $m = 2, 3, \dots, M - 1$  do
16:      $\mathbf{H}_{m, m-1} = -(q(x_{m+1}) * \sigma / (2\Delta x)) - (p(x_{m+1}) * \sigma / ((\Delta x)^2))$ 
17:      $\mathbf{H}_{m-1, m} = (q(x_{m+1}) * \sigma / (2\Delta x)) - (p(x_m) * \sigma / ((\Delta x)^2))$ 
18:   end for
19: end for
20: Output: Return of  $\mathbf{H}$ 

```

Algorithm 3 COMPUTATION OF $\tilde{\mathbf{H}}_{(M-1) \times (M-1)}$

```

1: Input 1:  $\alpha$  ▷ Order of the fractional operator
2: Input 2:  $M$  ▷ Number of mesh interval towards space
3: Input 3:  $N$  ▷ Number of mesh interval towards time
4: Compute  $\sigma = 1 - (\alpha/2)$ 
5: Compute  $\Delta x = L/M$  and  $\Delta t = T/N$  ▷ Mesh parameters
6: Compute  $x_m = m * \Delta x$  for  $m = 0, 1, \dots, M$ 
7: Compute  $t_n = n * \Delta t$  for  $m = 0, 1, \dots, N$ 
8: Compute  $p$  and  $q$  ▷ coefficient functions
9: Compute  $\mathcal{K}$  ▷ The given kernel
10: Compute  $d_0^1$  and  $d_j^{n+1}$  for  $n = 1, 2, \dots, N - 1, j = 0, 1, \dots, n - 1$  using Algorithm 1
11: for  $n = 1, 2, \dots, N$  do
12:   for  $m = 2, 3, \dots, M$  do
13:      $\tilde{\mathbf{H}}_{m-1, m-1} = d_n^{n+1} - (2 * p(x_m) * (1 - \sigma) / (\Delta x)^2) - (1 - \sigma) * q(x_m) - (\mu * \Delta t * \mathcal{K}(x_m, t_{n+\sigma} - t_n) / 2) -$   

 $(\mu * \sigma \Delta t * \mathcal{K}(x_m, t_{n+\sigma} - t_n) / 2) - (\mu * \Delta t * \sigma * (1 - \sigma) * \mathcal{K}(x_m, 0) / 2)$ 
14:   end for
15:   for  $m = 2, 3, \dots, M - 1$  do
16:      $\tilde{\mathbf{H}}_{m, m-1} = (q(x_{m+1}) * (1 - \sigma) / (2\Delta x)) + (p(x_{m+1}) * (1 - \sigma) / ((\Delta x)^2))$ 
17:      $\tilde{\mathbf{H}}_{m-1, m} = -(q(x_{m+1}) * (1 - \sigma) / (2\Delta x)) + (p(x_m) * (1 - \sigma) / ((\Delta x)^2))$ 
18:   end for
19: end for
20: Output: Return of  $\tilde{\mathbf{H}}$ 

```

Finally, we present the algorithm for solving the time-fraction integro-PDEs (1.1) described in Algorithm 4.

Algorithm 4 ALGORITHM FOR THE TIME-FRACTIONAL INTEGRO PDES

- 1: **Input 1:** α ▷ Order of the fractional operator
 - 2: **Input 2:** M ▷ Number of mesh interval towards space
 - 3: **Input 3:** N ▷ Number of mesh interval towards time
 - 4: **Input 4:** g, h_1, h_2 ▷ Initial and boundary conditions
 - 5: Compute $\sigma = 1 - (\alpha/2)$
 - 6: Compute $\Delta x = L/M$ and $\Delta t = T/N$ ▷ Mesh parameters
 - 7: Compute $x_m = m * \Delta x$ for $m = 0, 1, \dots, M$
 - 8: Compute $t_n = n * \Delta t$ for $m = 0, 1, \dots, N$
 - 9: Compute p and q ▷ coefficient functions
 - 10: Compute \mathcal{K} ▷ The given kernel
 - 11: Compute f
 - 12: Compute d_0^1 and d_j^{n+1} for $n = 1, 2, \dots, N - 1, j = 0, 1, \dots, n - 1$ using Algorithm 1
 - 13: **for** $n = 1, 2, \dots, N$ **do**
 - 14: Compute \mathbf{H} using Algorithm 2
 - 15: Compute $\tilde{\mathbf{H}}$ using Algorithm 3
 - 16: Compute the vector \mathcal{F}^n using steps 4, 7 and the formula given in (3.11)
 - 17: Compute $\mathcal{U}^{n+1} = \mathbf{H}^{-1}(\tilde{\mathbf{H}}\mathcal{U}^n + \mathcal{F}^n)$
 - 18: **end for**
 - 19: **Output:** Obtained discrete solution \mathcal{U}_m^n for $m = 1, 2, \dots, M - 1, n = 1, 2, \dots, N$
-

3.1.1. Discretization based on L1 scheme

The discrete scheme based on L1 discretization for the given problem (1.1) can be written as:

$$\left\{ \begin{array}{l} {}^{L1}\mathcal{D}_N^\alpha \mathcal{U}_m^n - p(x_m)\delta_{\Delta x}^2 \mathcal{U}_m^n + q(x_m)D_{\Delta x}^0 \mathcal{U}_m^n + r(x_m)\mathcal{U}_m^n \\ \quad + \frac{\mu\Delta t}{2} \sum_{j=0}^{n-1} [\mathcal{K}(x_m, t_n - t_{j+1})\mathcal{U}_m^{j+1} + \mathcal{K}(x_m, t_n - t_j)\mathcal{U}_m^j] = f(x_m, t_n) \\ \text{for } m = 1, 2, \dots, M - 1; n = 1, 2, \dots, N, \text{ with} \\ \mathcal{U}_m^0 = g(x_m) \text{ for } m = 0, 1, \dots, M, \\ \mathcal{U}_0^n = h_1(t_n) \text{ and } \mathcal{U}_M^n = h_2(t_n) \text{ for } n = 0, 1, \dots, N, \end{array} \right. \quad (3.13)$$

where

$$\left\{ \begin{array}{l} \partial_t^\alpha \mathcal{U}(x_m, t_n) \approx {}^{L1}\mathcal{D}_N^\alpha \mathcal{U}_m^n := \frac{1}{(\Delta t)^\alpha \Gamma(2 - \alpha)} \sum_{j=0}^{n-1} (\mathcal{U}_m^{j+1} - \mathcal{U}_m^j) \tilde{d}_{n-j}, \\ \frac{\partial^2 \mathcal{U}}{\partial x^2}(x_m, t_n) \approx \delta_{\Delta x}^2 \mathcal{U}_m^n := \frac{\mathcal{U}_{m+1}^n - 2\mathcal{U}_m^n + \mathcal{U}_{m-1}^n}{(\Delta x)^2}, \\ \frac{\partial \mathcal{U}}{\partial x}(x_m, t_n) \approx D_{\Delta x}^0 \mathcal{U}_m^n := \frac{\mathcal{U}_{m+1}^n - \mathcal{U}_{m-1}^n}{2\Delta x} \end{array} \right.$$

Here, $\tilde{d}_j = j^{1-\alpha} - (j-1)^{1-\alpha}$, $j \geq 1$. Further, $\int_0^{t_n} \mathcal{K}(x_m, t_n - \xi)\mathcal{U}(x_m, \xi) d\xi \approx \frac{\Delta t}{2} \sum_{j=0}^{n-1} [\mathcal{K}(x_m, t_n - t_{j+1})\mathcal{U}(x_m, t_{j+1}) + \mathcal{K}(x_m, t_n - t_j)\mathcal{U}(x_m, t_j)]$. The discrete scheme (3.13) has the truncation error

$${}^{L1}\mathcal{R}_m^n = \left(\partial_t^\alpha - {}^{L1}\mathcal{D}_N^\alpha \right) \mathcal{U}(x_m, t_n) + O((\Delta t)^2 + (\Delta x)^2). \quad (3.14)$$

3.2. Approximation of two-dimensional integro-PDEs

In this segment, we discuss the approximation scheme for two-dimensional integro-PDEs depicted in (1.2) based on the $L2-1_\sigma$ scheme and the Haar wavelets. First, we make the semi-discretization of the model by using the $L2-1_\sigma$ scheme for the fractional operator, and the composite trapezoidal approximation for the Volterra integral operator. The Wavelet collocation method is then applied to solve the semi-discrete problem.

3.2.1. The temporal semi-discretization

The temporal direction is discretized uniformly as described in Section 3.1. In a similar way as defined in (3.2), the Caputo fractional operator presented in (1.2) is approximated at the nodal point $t_{n+\sigma}$ as:

$$\partial_t^\alpha \mathcal{U}(\cdot, t_{n+\sigma}) \approx {}^{L2-1_\sigma} \mathcal{D}_N^\alpha \mathcal{U}^{n+\sigma} := \sum_{j=0}^n d_j^{n+1} (\mathcal{U}^{j+1} - \mathcal{U}^j), \quad (3.15)$$

where d_j^{n+1} is defined in (3.3). The Volterra operator is discretized in a similar way as defined in (3.6), given by:

$$\begin{aligned} \int_0^{t_{n+\sigma}} \mathcal{K}(\cdot, t_{n+\sigma} - \xi) \mathcal{U}(\cdot, \xi) d\xi &\approx \frac{\Delta t}{2} \sum_{j=0}^{n-1} [\mathcal{K}(\cdot, t_{n+\sigma} - t_{j+1}) \mathcal{U}^{j+1} + \mathcal{K}(\cdot, t_{n+\sigma} - t_j) \mathcal{U}^j] \\ &+ \frac{\sigma \Delta t}{2} \mathcal{K}(\cdot, t_{n+\sigma} - t_n) \mathcal{U}^n + \frac{\sigma \Delta t}{2} \mathcal{K}(\cdot, 0) [\sigma \mathcal{U}^{n+1} + (1 - \sigma) \mathcal{U}^n] + O((\Delta t)^2). \end{aligned} \quad (3.16)$$

Therefore, the temporal discretization of (1.2) is given by:

$$\begin{cases} \left(d_n^{n+1} + \frac{\mu \sigma^2 \Delta t}{2} \mathcal{K}(x, y, 0) \right) \mathcal{U}^{n+1}(x, y) - \mathfrak{L}^N \mathcal{U}^{n+\sigma}(x, y) = F^n(x, y), \\ \mathcal{U}^{n+\sigma}(0, y) = h_1(y, t_{n+\sigma}) \text{ and } \mathcal{U}^{n+\sigma}(1, y) = h_2(y, t_{n+\sigma}), \\ \mathcal{U}^{n+\sigma}(x, 0) = h_3(x, t_{n+\sigma}) \text{ and } \mathcal{U}^{n+\sigma}(x, 1) = h_4(x, t_{n+\sigma}) \quad \forall n = 0, 1, \dots, N-1, \end{cases} \quad (3.17)$$

where \mathfrak{L}^N and $F^n(x, y)$ are given by:

$$\begin{aligned} \mathfrak{L}^N \mathcal{U}^{n+\sigma}(x, y) &= p_1(x, y) \mathcal{U}_{xx}^{n+\sigma}(x, y) + p_2(x, y) \mathcal{U}_{yy}^{n+\sigma}(x, y) - q_1(x, y) \mathcal{U}_x^{n+\sigma}(x, y) \\ &\quad - q_2(x, y) \mathcal{U}_y^{n+\sigma}(x, y) - r_1(x, y) \mathcal{U}^{n+\sigma}(x, y), \\ F^n(x, y) &= \left(d_n^{n+1} - \frac{\mu \sigma (1 - \sigma) \Delta t}{2} \mathcal{K}(x, y, 0) \right) \mathcal{U}^n(x, y) - \sum_{j=0}^{n-1} d_j^{n+1} (\mathcal{U}^{j+1}(x, y) - \mathcal{U}^j(x, y)) \\ &\quad - \frac{\mu \sigma \Delta t}{2} \mathcal{K}(x, y, t_{n+\sigma} - t_n) \mathcal{U}^n(x, y) - \frac{\mu \Delta t}{2} \sum_{j=0}^{n-1} \left[\mathcal{K}(x, y, t_{n+\sigma} - t_{j+1}) \mathcal{U}^{j+1}(x, y) \right. \\ &\quad \left. + \mathcal{K}(x, y, t_{n+\sigma} - t_j) \mathcal{U}^j(x, y) \right] + f(x, y, t_{n+\sigma}). \end{aligned}$$

3.2.2. Approximation of spatial derivatives based on Haar wavelets

In this segment, we present the complete solution of (1.2) by solving the semi-discretized problem given in (3.17) using the Haar wavelets. The Haar wavelet [36, 37] consists of a sequence of square-shaped functions that together form a wavelet family. The mother wavelet function $\psi(x)$, and its

scaling function $\phi(x)$ is defined as:

$$\psi(x) = \begin{cases} 1, & \text{for } t \in \left[0, \frac{1}{2}\right), \\ -1, & \text{for } t \in \left[\frac{1}{2}, 1\right), \\ 0, & \text{elsewhere,} \end{cases} \quad \text{and} \quad \phi(x) = \begin{cases} 1, & \text{for } t \in [0, 1), \\ 0, & \text{elsewhere.} \end{cases}$$

The corresponding basis functions can be generated by using the dilation parameter j and the translation parameter k as: $\{\phi_k^j(x) = 2^{j/2}\phi(2^j x - k)\}_{j,k \in \mathbb{Z}}$, $\{\psi_k^j(x) = 2^{j/2}\psi(2^j x - k)\}_{j,k \in \mathbb{Z}}$ to form an orthonormal subfamily of the Hilbert space $L^2(\mathbb{R})$. Let us choose $i = m + k + 1$, where $m = 2^j$ for $j = 0, 1, \dots, J$ and $k = 0, 1, \dots, m - 1$. Then, for $t \in [0, 1]$, the i^{th} Haar wavelet is defined as:

$$\psi_i(x) = \begin{cases} 1, & \text{for } x \in [\zeta_1(i), \zeta_2(i)), \\ -1, & \text{for } x \in [\zeta_2(i), \zeta_3(i)), \quad i = 2, 3, \dots, \\ 0, & \text{elsewhere,} \end{cases} \quad (3.18)$$

where $\zeta_1(i) = \frac{k}{m}$, $\zeta_2(i) = \frac{k+1/2}{m}$, $\zeta_3(i) = \frac{k+1}{m}$. J is called the maximum level of resolution. Further, the n^{th} , $n \in \mathbb{N}$ integration of the Haar wavelets can be written as:

$$\mathcal{R}_{n,1}(x) = \frac{x^n}{n!}, \quad \text{for all } x \in [0, 1),$$

and for $i = 2, 3, \dots$,

$$\mathcal{R}_{n,i}(x) = \frac{1}{n!} \begin{cases} 0, & 0 \leq x < \zeta_1(i), \\ (x - \zeta_1(i))^n, & \zeta_1(i) \leq x < \zeta_2(i), \\ (x - \zeta_1(i))^n - 2(x - \zeta_2(i))^n, & \zeta_2(i) \leq x < \zeta_3(i), \\ (x - \zeta_1(i))^n - 2(x - \zeta_2(i))^n + (x - \zeta_3(i))^n, & \zeta_3(i) \leq x < 1. \end{cases}$$

A real-valued function $z(x, y) \in L^2([0, 1] \times [0, 1])$ can be approximated using two-dimensional Haar wavelets as:

$$\begin{aligned} z(x, y) &\approx D_{1,1}\phi(x)\phi(y) + \sum_{i_2=2}^{2M_2} D_{1,i_2}\phi(x)\psi_{i_2}(y) + \sum_{i_1=2}^{2M_1} D_{i_1,1}\psi_{i_1}(x)\phi(y) + \sum_{i_1=2}^{2M_1} \sum_{i_2=2}^{2M_2} D_{i_1,i_2}\psi_{i_1}(x)\psi_{i_2}(y) \\ &= \mathcal{H}(x)^T \mathbf{D} \mathcal{H}(y), \end{aligned}$$

where $\mathcal{H}(x) = (\phi(x), \psi_2(x), \dots, \psi_{2M_1}(x))^T$, $\mathcal{H}(y) = (\phi(y), \psi_2(y), \dots, \psi_{2M_2}(y))^T$, and \mathbf{D} is the matrix of unknown coefficients of order $(2M_1 \times 2M_2)$, given by:

$$\mathbf{D} = \begin{pmatrix} D_{1,1} & D_{1,2} & \cdots & D_{1,2M_2} \\ D_{2,1} & D_{2,2} & \cdots & D_{2,2M_2} \\ \vdots & \vdots & \ddots & \vdots \\ D_{2M_1,1} & D_{2M_1,2} & \cdots & D_{2M_1,2M_2} \end{pmatrix}.$$

Here, we take $i_1 = m_1 + k_1 + 1$, with $m_1 = 2^{j_1}$ for $j_1 = 0, 1, \dots, J_1$ and $k_1 = 0, 1, \dots, m_1 - 1$. $i_2 = m_2 + k_2 + 1$, with $m_2 = 2^{j_2}$ for $j_2 = 0, 1, \dots, J_2$ and $k_2 = 0, 1, \dots, m_2 - 1$. J_1 and J_2 represent the

maximum level of resolution in the direction of x and y , respectively. Further, $M_1 = 2^{J_1}$, $M_2 = 2^{J_2}$. In order to find the unknown matrix, we use the two-dimensional collocation points $\{(x_{l_1}, y_{l_2})\}_{l_1=1, l_2=1}^{2M_1, 2M_2}$ defined as:

$$x_{l_1} = \frac{l_1 - 1/2}{2M_1}, \quad y_{l_2} = \frac{l_2 - 1/2}{2M_2}, \quad l_1 = 1, 2, \dots, 2M_1, \quad l_2 = 1, 2, \dots, 2M_2. \quad (3.19)$$

Let us assume $\mathcal{U}_{xxyy}^{n+\sigma}(x, y) \in L^2([0, 1] \times [0, 1])$. Then, $\mathcal{U}_{xxyy}^{n+\sigma}(x, y)$ can be approximated as:

$$\mathcal{U}_{xxyy}^{n+\sigma}(x, y) \approx \mathcal{H}(x)^T \mathbf{D} \mathcal{H}(y). \quad (3.20)$$

Integrating (3.20) with respect to y two times and then, using the boundary conditions given in (3.17), we get

$$\mathcal{U}_{xx}^{n+\sigma}(x, y) \approx \mathcal{H}(x)^T \mathbf{D} (\mathcal{R}_2(y) - y \mathcal{R}_2(1)) + (1 - y) \frac{\partial^2 h_3}{\partial x^2}(x, t_{n+\sigma}) + y \frac{\partial^2 h_4}{\partial x^2}(x, t_{n+\sigma}), \quad (3.21)$$

where $\mathcal{R}_2(y) := (\mathcal{R}_{2,1}(y), \mathcal{R}_{2,2}(y), \dots, \mathcal{R}_{2,2M_2}(y))^T$. Again, integrating (3.20) with respect to x two times and then, using the boundary conditions, we yield

$$\mathcal{U}_{yy}^{n+\sigma}(x, y) \approx (\mathcal{R}_2(x) - x \mathcal{R}_2(1))^T \mathbf{D} \mathcal{H}(y) + (1 - x) \frac{\partial^2 h_1}{\partial y^2}(y, t_{n+\sigma}) + x \frac{\partial^2 h_2}{\partial y^2}(y, t_{n+\sigma}), \quad (3.22)$$

with $\mathcal{R}_2(x) := (\mathcal{R}_{2,1}(x), \mathcal{R}_{2,2}(x), \dots, \mathcal{R}_{2,2M_1}(x))^T$. Further, the integration of (3.21) with respect to x two times consequently, and the integration of (3.22) with respect to y one time, yields the following:

$$\begin{aligned} \mathcal{U}_x^{n+\sigma}(x, y) &\approx (\mathcal{R}_1(x) - \mathcal{R}_2(1))^T \mathbf{D} (\mathcal{R}_2(y) - y \mathcal{R}_2(1)) - h_1(y, t_{n+\sigma}) + h_2(y, t_{n+\sigma}) \\ &\quad + (1 - y) \left(\frac{\partial h_3}{\partial x}(x, t_{n+\sigma}) - h_3(1, t_{n+\sigma}) + h_3(0, t_{n+\sigma}) \right) \\ &\quad + y \left(\frac{\partial h_4}{\partial x}(x, t_{n+\sigma}) - h_4(1, t_{n+\sigma}) + h_4(0, t_{n+\sigma}) \right), \end{aligned} \quad (3.23)$$

$$\begin{aligned} \mathcal{U}_y^{n+\sigma}(x, y) &\approx (\mathcal{R}_2(x) - x \mathcal{R}_2(1))^T \mathbf{D} (\mathcal{R}_1(y) - \mathcal{R}_2(1)) - h_3(x, t_{n+\sigma}) + h_4(x, t_{n+\sigma}) \\ &\quad + (1 - x) \left(\frac{\partial h_1}{\partial y}(y, t_{n+\sigma}) - h_1(1, t_{n+\sigma}) + h_1(0, t_{n+\sigma}) \right) \\ &\quad + x \left(\frac{\partial h_2}{\partial y}(y, t_{n+\sigma}) - h_2(1, t_{n+\sigma}) + h_2(0, t_{n+\sigma}) \right), \end{aligned} \quad (3.24)$$

$$\begin{aligned} \mathcal{U}^{n+\sigma}(x, y) &\approx (\mathcal{R}_2(x) - x \mathcal{R}_2(1))^T \mathbf{D} (\mathcal{R}_2(y) - y \mathcal{R}_2(1)) + (1 - x) h_1(y, t_{n+\sigma}) + x h_2(y, t_{n+\sigma}) \\ &\quad + (1 - y) (h_3(x, t_{n+\sigma}) - h_3(0, t_{n+\sigma}) - x h_3(1, t_{n+\sigma}) + x h_3(0, t_{n+\sigma})) \\ &\quad + y (h_4(x, t_{n+\sigma}) - h_4(0, t_{n+\sigma}) - x h_4(1, t_{n+\sigma}) + x h_4(0, t_{n+\sigma})), \end{aligned} \quad (3.25)$$

where $\mathcal{R}_1(x) := (\mathcal{R}_{1,1}(x), \mathcal{R}_{1,2}(x), \dots, \mathcal{R}_{1,2M_1}(x))^T$, $\mathcal{R}_1(y) := (\mathcal{R}_{1,1}(y), \mathcal{R}_{1,2}(y), \dots, \mathcal{R}_{1,2M_2}(y))^T$. Using Lemma 3.1 in (3.25), we have

$$\begin{aligned} \mathcal{U}^{n+1}(x, y) &\approx \frac{1}{\sigma} \left[(\mathcal{R}_2(x) - x \mathcal{R}_2(1))^T \mathbf{D} (\mathcal{R}_2(y) - y \mathcal{R}_2(1)) + (1 - x) h_1(y, t_{n+\sigma}) + x h_2(y, t_{n+\sigma}) \right. \\ &\quad + (1 - y) (h_3(x, t_{n+\sigma}) - h_3(0, t_{n+\sigma}) - x h_3(1, t_{n+\sigma}) + x h_3(0, t_{n+\sigma})) \\ &\quad \left. + y (h_4(x, t_{n+\sigma}) - h_4(0, t_{n+\sigma}) - x h_4(1, t_{n+\sigma}) + x h_4(0, t_{n+\sigma})) \right] - \left(\frac{1 - \sigma}{\sigma} \right) \mathcal{U}^n(x, y), \end{aligned} \quad (3.26)$$

Substituting (3.21)-(3.26) into (3.17), one can have a linear system at each time level and that can be solved by using the collocation points defined in (3.19). Then, after substituting the wavelet

coefficients into (3.26), we get the numerical solution of (1.2) at each time level.

Note 1: The one-dimensional time-fractional integro-PDE (1.1) can also be solved by using the semi-discretization technique described in Section 3.2.1. In that case, we need to apply the one-dimensional Haar wavelet approximation to approximate the spatial derivatives.

4. Stability and convergence analysis

In this section, we will show that the proposed method is unconditionally stable, and gives a higher rate of convergence for solving time-fractional integro PDEs of type (1.1). In order to obtain the required results, we need the following truncation error bound for $L2-1_\sigma$ scheme for approximating time-fractional operator given in [27].

Lemma 4.1. *Let $\alpha \in (0, 1)$ and $\mathcal{U} \in C^3(\bar{\Omega}, \mathbb{R})$. Then, for any $(x_m, t_n) \in \Omega_{M,N}$, we have*

$$\left| (\partial_t^\alpha - {}^{L2-1_\sigma}\mathcal{D}_N^\alpha) \mathcal{U}(x_m, t_n) \right| \leq C(\Delta t)^{3-\alpha}.$$

Lemma 4.2. [27] *For $n = 0, 1, \dots, N-1$, if $d_n^{n+1} > d_{n-1}^{n+1} > \dots > d_0^{n+1} > 0$ and $\frac{d_n^{n+1}}{2d_n^{n+1} - d_{n-1}^{n+1}} \leq \sigma \leq 1$ with $d_{-1}^1 = 0$, then one has*

$$(\sigma \mathcal{U}^{n+1} + (1 - \sigma) \mathcal{U}^n) {}^{L2-1_\sigma}\mathcal{D}_N^\alpha \mathcal{U}^{n+\sigma} \geq \frac{1}{2} {}^{L2-1_\sigma}\mathcal{D}_N^\alpha (\mathcal{U}^{n+\sigma})^2.$$

Let us consider the following discrete problem with homogeneous boundary conditions:

$$\begin{cases} {}^{L2-1_\sigma}\mathcal{D}_N^\alpha \mathcal{U}_m^{n+\sigma} - p(x_m) \delta_{\Delta x, \Delta t}^2 \mathcal{U}_m^{n+\sigma} + q(x_m) D_{\Delta x, \Delta t}^0 \mathcal{U}_m^{n+\sigma} \\ \quad + r(x_m) \mathcal{U}_m^{n+\sigma} + \mu \mathcal{I}_N \mathcal{U}_m^{n+\sigma} = f(x_m, t_{n+\sigma}), \\ \text{for } m = 1, 2, \dots, M-1; n = 0, 1, \dots, N-1, \\ \mathcal{U}_m^0 = g(x_m) \text{ for } m = 0, 1, \dots, M, \\ \mathcal{U}_0^n = \mathcal{U}_M^n = 0 \text{ for } n = 0, 1, \dots, N. \end{cases} \quad (4.1)$$

For any mesh functions $\left\{ \mathcal{U}_m^n \right\}_{m=0, n=0}^{M, N}$, $\left\{ \mathcal{V}_m^n \right\}_{m=0, n=0}^{M, N}$, let us define $\|\mathcal{U}^n\| = \sqrt{\langle \mathcal{U}^n, \mathcal{U}^n \rangle}$, $\|\mathcal{U}\| = \max_{0 \leq n \leq N} \|\mathcal{U}^n\|$, where $\langle \mathcal{U}, \mathcal{V} \rangle = \sum_{m=1}^{M-1} \mathcal{U}_m \mathcal{V}_m$.

Theorem 4.3. *The solution of the discrete problem (4.1) satisfies the following inequality*

$$\left\| \mathcal{U}^{n+1} \right\|^2 \leq \left\| \mathcal{U}^0 \right\|^2 + \frac{L^2 T^\alpha \Gamma(1-\alpha)}{4p_0^2 + r_0 L^2} \max_{0 \leq n \leq N} \left\| f^{n+\sigma} \right\|^2, \quad n = 0, 1, \dots, N-1,$$

provided $d_n^{n+1} > d_{n-1}^{n+1} > \dots > d_0^{n+1} \geq \mathcal{C} > 0$, and $\frac{d_n^{n+1}}{2d_n^{n+1} - d_{n-1}^{n+1}} \leq \sigma \leq 1$ for all $n = 0, 1, \dots, N-1$

with $\mathcal{C} = \frac{1}{2T^\alpha \Gamma(1-\alpha)}$ and $d_{-1}^1 = 0$.

Proof. Keeping in mind of positive definiteness of the operators $-\delta_{\Delta x, \Delta t}^2$, $D_{\Delta x, \Delta t}^0$ and \mathcal{I}_N , we have $\langle -p \delta_{\Delta x, \Delta t}^2 \mathcal{U}, \mathcal{U} \rangle \geq \frac{4p_0}{L^2} \|\mathcal{U}\|^2$, $\langle D_{\Delta x, \Delta t}^0 \mathcal{U}, \mathcal{U} \rangle \geq 0$, and $\langle \mathcal{I}_N \mathcal{U}, \mathcal{U} \rangle \geq 0$. Taking the inner product

of (4.1) with $\mathcal{U}^{n+\sigma}$ to yield

$$\begin{aligned} & \langle \mathcal{U}^{n+\sigma}, L^{2-1\sigma} \mathcal{D}_N^\alpha \mathcal{U}^{n+\sigma} \rangle + \langle \mathcal{U}^{n+\sigma}, -p\delta_{\Delta x, \Delta t}^2 \mathcal{U}^{n+\sigma} \rangle + \langle \mathcal{U}^{n+\sigma}, qD_{\Delta x, \Delta t}^0 \mathcal{U}^{n+\sigma} \rangle \\ & + \langle \mathcal{U}^{n+\sigma}, r\mathcal{U}^{n+\sigma} \rangle + \mu \langle \mathcal{U}^{n+\sigma}, \mathcal{J}_N \mathcal{U}^{n+\sigma} \rangle = \langle \mathcal{U}^{n+\sigma}, f^{n+\sigma} \rangle \end{aligned}$$

Use Lemma 4.2 to get

$$\frac{1}{2} L^{2-1\sigma} \mathcal{D}_N^\alpha \left\| \mathcal{U}^{n+\sigma} \right\|^2 + \frac{4p_0^2}{L^2} \left\| \mathcal{U}^{n+\sigma} \right\|^2 + r_0 \left\| \mathcal{U}^{n+\sigma} \right\|^2 \leq \varepsilon \left\| \mathcal{U}^{n+\sigma} \right\|^2 + \frac{1}{4\varepsilon} \left\| f^{n+\sigma} \right\|^2.$$

Notice that the kernel \mathcal{K} is positive real-valued, and taking $\varepsilon = \left(\frac{4p_0^2}{L^2} + r_0 \right)$, one can write

$$\begin{aligned} L^{2-1\sigma} \mathcal{D}_N^\alpha \left\| \mathcal{U}^{n+\sigma} \right\|^2 & \leq \frac{L^2}{2(4p_0^2 + r_0 L^2)} \left\| f^{n+\sigma} \right\|^2 \\ \Rightarrow d_n^{n+1} \left\| \mathcal{U}^{n+1} \right\|^2 & \leq \sum_{j=1}^n (d_j^{n+1} - d_{j-1}^{n+1}) \left\| \mathcal{U}^j \right\|^2 + d_0^{n+1} \left\| \mathcal{U}^0 \right\|^2 + \frac{L^2}{2(4p_0^2 + r_0 L^2)} \left\| f^{n+\sigma} \right\|^2 \\ & \leq \sum_{j=1}^n (d_j^{n+1} - d_{j-1}^{n+1}) \left\| \mathcal{U}^j \right\|^2 + d_0^{n+1} \left(\left\| \mathcal{U}^0 \right\|^2 + \frac{L^2 T^\alpha \Gamma(1-\alpha)}{4p_0^2 + r_0 L^2} \left\| f^{n+\sigma} \right\|^2 \right). \end{aligned} \quad (4.2)$$

Let us take $\mathcal{D} = \left\| \mathcal{U}^0 \right\|^2 + \frac{L^2 T^\alpha \Gamma(1-\alpha)}{4p_0^2 + r_0 L^2} \max_{0 \leq n \leq N} \left\| f^{n+\sigma} \right\|^2$. Now, we will use mathematical induction to prove the theorem. For $n = 0$, the theorem is automatically satisfied from (4.2). Let us assume that the inequality holds true for $n = 1, 2, \dots, k-1$, i.e. $\left\| \mathcal{U}^{n+1} \right\|^2 \leq \mathcal{D}$, $n = 1, \dots, k-1$. Now, from (4.2), we have

$$\begin{aligned} d_k^{k+1} \left\| \mathcal{U}^{k+1} \right\|^2 & \leq \sum_{j=1}^k (d_j^{k+1} - d_{j-1}^{k+1}) \left\| \mathcal{U}^j \right\|^2 + d_0^{k+1} \mathcal{D} \leq \sum_{j=1}^k (d_j^{k+1} - d_{j-1}^{k+1}) \mathcal{D} + d_0^{k+1} \mathcal{D} = d_k^{k+1} \mathcal{D} \\ \Rightarrow \left\| \mathcal{U}^{k+1} \right\|^2 & \leq \mathcal{D} = \left\| \mathcal{U}^0 \right\|^2 + \frac{L^2 T^\alpha \Gamma(1-\alpha)}{4p_0^2 + r_0 L^2} \max_{0 \leq n \leq N} \left\| f^{n+\sigma} \right\|^2. \end{aligned}$$

Hence, the theorem is proved. \square

The error equation can be obtained by subtracting (3.9) from (3.7) as follows:

$$\begin{cases} L^{2-1\sigma} \mathcal{D}_N^\alpha e_m^{n+\sigma} - p(x_m) \delta_{\Delta x, \Delta t}^2 e_m^{n+\sigma} + q(x_m) D_{\Delta x, \Delta t}^0 e_m^{n+\sigma} + r(x_m) e_m^{n+\sigma} + \mu \mathcal{J}_N e_m^{n+\sigma} = L^{2-1\sigma} \mathcal{R}_m^{n+\sigma}, \\ \text{for } m = 1, 2, \dots, M-1; n = 0, 1, \dots, N-1, \\ e_m^0 = 0 \text{ for } m = 0, 1, \dots, M, \\ e_0^n = e_M^n = 0 \text{ for } n = 0, 1, \dots, N, \end{cases} \quad (4.3)$$

where $L^{2-1\sigma} \mathcal{R}_m^{n+\sigma}$ is the remainder term defined in (3.8), and $e_m^{n+\sigma} = \mathcal{U}(x_m, t_{n+\sigma}) - \mathcal{U}_m^{n+\sigma}$.

4.1. Convergence based on L2-1 σ scheme

Theorem 4.4. *If (1.1) has a solution $\mathcal{U} \in C_{x,t}^{4,3}(\bar{\Omega}, \mathbb{R})$ and let $\{\mathcal{U}(x_m, t_n)\}_{m=0, n=0}^{M, N}$ and $\{\mathcal{U}_m^n\}_{m=0, n=0}^{M, N}$ be the exact and the numerical solution of (1.1) by using the discrete scheme (3.9), respectively. Then, one has the following error bound:*

$$\|e\| \leq C [(\Delta t)^{3-\alpha} + (\Delta t)^2 + (\Delta x)^2].$$

Proof. Theorem 4.3 implies that the solution of the discrete problem (4.3) satisfies the following bound for $n = 0, 1, \dots, N - 1$.

$$\begin{aligned} \left\| e^{n+1} \right\|^2 &\leq \left\| e^0 \right\|^2 + \frac{L^2 T^\alpha \Gamma(1 - \alpha)}{4p_0^2 + r_0 L^2} \max_{0 \leq n \leq N} \left\| {}^{L2-1_\sigma} \mathcal{R}^{n+\sigma} \right\|^2 \\ \Rightarrow \left\| e^{n+1} \right\| &\leq \sqrt{\frac{L^2 T^\alpha \Gamma(1 - \alpha)}{4p_0^2 + r_0 L^2}} \max_{0 \leq n \leq N} \left\| {}^{L2-1_\sigma} \mathcal{R}^{n+\sigma} \right\| \\ &\leq C \max_{0 \leq n \leq N} \left\| \left(\partial_t^\alpha - {}^{L2-1_\sigma} \mathcal{D}_N^\alpha \right) \mathcal{U}^{n+\sigma} \right\| + O((\Delta t)^2 + (\Delta x)^2). \end{aligned}$$

Now, using Lemma 4.1, we get

$$\|e\| = \max_{0 \leq n \leq N-1} \left\| e^{n+1} \right\| \leq C [(\Delta t)^{3-\alpha} + (\Delta t)^2 + (\Delta x)^2]$$

□

Note 2: For $L2-1_\sigma$ scheme, it can be observed that the truncation error bound $O((\Delta t)^{3-\alpha})$ corresponding to the fractional operator is dominated by the truncation error bound $O((\Delta t)^2)$, and hence the proposed scheme overall gives a second-order convergence for any values of $\alpha \in (0, 1)$ (see Tables 1, 2, 3, 4 of Section 5).

Lemma 4.5. If $\mathcal{U} \in C^2(\bar{\Omega}, \mathbb{R})$, the truncation error corresponding to the $L1$ scheme satisfies the following bound:

$$\left| \left(\partial_t^\alpha - {}^{L1} \mathcal{D}_N^\alpha \right) \mathcal{U}(x_m, t_n) \right| \leq C(\Delta t)^{2-\alpha}, \text{ for } (x_m, t_n) \in \Omega_{M,N}. \quad (4.4)$$

Proof. A similar kind of proof is available in [25, 38].

□

4.2. Convergence based on $L1$ scheme

Theorem 4.6. If (1.1) has a solution in $C_{x,t}^{4,2}(\bar{\Omega}, \mathbb{R})$, then, the solution of the discrete problem (3.13) converges to the exact solution of (1.1) with an error \tilde{e}_m^n , $m = 0, 1, \dots, M$; $n = 0, 1, \dots, N$, satisfying the following bound with respect to the L_∞ -norm.

$$\|\tilde{e}\|_\infty \leq C [(\Delta t)^{2-\alpha} + (\Delta t)^2 + (\Delta x)^2].$$

Proof. The proof of this lemma is available in [39] for a time-fractional diffusion equation and it can be extended by introducing the truncation error bound $O((\Delta t)^2)$, occurred due to the presence of the Volterra integral operator.

□

Note 3: In the case of $L1$ scheme, the truncation error bounds corresponding to the integral operator as well as the spatial derivative are dominated by the truncation error bound $O((\Delta t)^{2-\alpha})$ occurred due to the discretization of fractional operator, where $\alpha \in (0, 1)$. Hence, the $L1$ scheme globally gives a $2 - \alpha$ rate of convergence. Also, see Tables 2, 3, 4 at Section 5.

Remark 1. For α tends to 1, it can be observed that the $L1$ scheme gives almost 1st order convergence rate whereas, the $L2-1_\sigma$ scheme produces 2nd order accuracy for the given problem (1.1) (see also the Tables 2, 3, 4 of Section 5).

4.3. Convergence based on two-dimensional Haar wavelets

In this section, our objective is to demonstrate the convergence of the numerical approximation based on two-dimensional Haar wavelets by using their orthogonality property given by

$$\int_0^1 \psi_{i_1}(x)\psi_{i'_1}(x) dx = \begin{cases} \frac{1}{2M_1}, & \text{if } i_1 = i'_1, \\ 0, & \text{if } i_1 \neq i'_1 \end{cases}, \quad \int_0^1 \psi_{i_2}(y)\psi_{i'_2}(y) dy = \begin{cases} \frac{1}{2M_2}, & \text{if } i_2 = i'_2, \\ 0, & \text{if } i_2 \neq i'_2 \end{cases}.$$

Again, we have

$$\mathcal{U}_{\text{Exact}}(x, y) - \mathcal{U}_{\text{Numer.}}(x, y) = \sum_{i_1=2M_1+1}^{\infty} \sum_{i_2=2M_2+1}^{\infty} D_{i_1, i_2} \psi_{i_1}(x)\psi_{i_2}(y), \quad (4.5)$$

where $\mathcal{U}_{\text{Exact}}$ and $\mathcal{U}_{\text{Numer.}}$ denote the exact and numerical solution by using two-dimensional Haar wavelets.

Theorem 4.7. *Suppose that $\mathcal{U}(x, t) \in L^2([0, 1] \times [0, 1])$ such that $\left| \frac{\partial \mathcal{U}}{\partial x} \right| \leq \mathcal{M}$, for all $(x, t) \in [0, 1] \times [0, 1]$, for some $\mathcal{M} \in \mathbb{N}$. Then, we have the following bound.*

$$\left\| \mathcal{U}_{\text{Exact}}(x, y) - \mathcal{U}_{\text{Numer.}}(x, y) \right\|_{L^2} \leq \frac{\mathcal{M}}{12(M_1 M_2)^{3/2}},$$

where $\|\mathcal{U}(x, y)\|_{L^2}^2 = \int_0^1 \int_0^1 (\mathcal{U}(x, y))^2 dx dy$. In particular, the numerical solution converges, i.e., $\left\| \mathcal{U}_{\text{Exact}}(x, y) - \mathcal{U}_{\text{Numer.}}(x, y) \right\|_{L^2} \rightarrow 0$ as $M_1 \rightarrow \infty$, $M_2 \rightarrow \infty$.

Proof. The idea that we have used to prove this theorem has been used in [40]. Taking square of the norm $\|\cdot\|_{L^2}$ applied on the both sides of (4.5), and using orthogonality property, we yield

$$\begin{aligned} \left\| \mathcal{U}_{\text{Exact}}(x, y) - \mathcal{U}_{\text{Numer.}}(x, y) \right\|_{L^2}^2 &= \int_0^1 \int_0^1 (\mathcal{U}_{\text{Exact}}(x, y) - \mathcal{U}_{\text{Numer.}}(x, y))^2 dx dy \\ &= \sum_{i_1=2M_1+1}^{\infty} \sum_{i_2=2M_2+1}^{\infty} \sum_{i'_1=2M_1+1}^{\infty} \sum_{i'_2=2M_2+1}^{\infty} D_{i_1, i_2, i'_1, i'_2} \left(\int_0^1 \psi_{i_1}(x)\psi_{i'_1}(x) dx \right) \left(\int_0^1 \psi_{i_2}(y)\psi_{i'_2}(y) dy \right) \\ &= \frac{1}{4M_1 M_2} \sum_{i_1=2M_1+1}^{\infty} \sum_{i_2=2M_2+1}^{\infty} D_{i_1, i_2}^2, \end{aligned} \quad (4.6)$$

where $D_{i_1, i_2} = \langle \psi_{i_1}(x), \langle \mathcal{U}(x, y), \psi_{i_2}(y) \rangle \rangle$. Following (3.18), and applying the Mean Value Theorem for integrals, one has

$$\begin{aligned} \langle \mathcal{U}(x, y), \psi_{i_2}(y) \rangle &= \int_0^1 \mathcal{U}(x, y)\psi_{i_2}(y) dy = \int_{k_2/2^{j_2}}^{(k_2+\frac{1}{2})/2^{j_2}} \mathcal{U}(x, y) dy - \int_{(k_2+\frac{1}{2})/2^{j_2}}^{(k_2+1)/2^{j_2}} \mathcal{U}(x, y) dy \\ &= 2^{-(j_2+1)} (\mathcal{U}(x, y_1) - \mathcal{U}(x, y_2)), \end{aligned}$$

for some $\frac{k_2}{2^{j_2}} < y_1 < \frac{k_2 + \frac{1}{2}}{2^{j_2}}$, $\frac{k_2 + \frac{1}{2}}{2^{j_2}} < y_2 < \frac{k_2 + 1}{2^{j_2}}$. Therefore,

$$\begin{aligned}
D_{i_1, i_2} &= \langle \psi_{i_1}(x), \langle \mathcal{U}(x, y), \psi_{i_2}(y) \rangle \rangle = 2^{-(j_2+1)} \int_0^1 \psi_{i_1}(x) \mathcal{U}(x, y_1) dx - 2^{-(j_2+1)} \int_0^1 \psi_{i_1}(x) \mathcal{U}(x, y_2) dx \\
&= 2^{-(j_2+1)} \left(\int_{k_1/2^{j_1}}^{(k_1+\frac{1}{2})/2^{j_1}} \mathcal{U}(x, y_1) dx - \int_{(k_1+\frac{1}{2})/2^{j_1}}^{(k_1+1)/2^{j_1}} \mathcal{U}(x, y_1) dx \right) \\
&\quad - 2^{-(j_2+1)} \left(\int_{k_1/2^{j_1}}^{(k_1+\frac{1}{2})/2^{j_1}} \mathcal{U}(x, y_2) dx - \int_{(k_1+\frac{1}{2})/2^{j_1}}^{(k_1+1)/2^{j_1}} \mathcal{U}(x, y_2) dx \right) \\
&= 2^{-(j_1+j_2+2)} (\mathcal{U}(x_1, y_1) - \mathcal{U}(x_2, y_1)) - 2^{-(j_1+j_2+2)} (\mathcal{U}(x_3, y_2) - \mathcal{U}(x_4, y_2)),
\end{aligned}$$

where $\frac{k_1}{2^{j_1}} < x_1, x_3 < \frac{k_1 + \frac{1}{2}}{2^{j_1}}$, $\frac{k_1 + \frac{1}{2}}{2^{j_1}} < x_2, x_4 < \frac{k_1 + 1}{2^{j_1}}$. Further, using Lagrange Mean Value Theorem, we yield

$$\begin{aligned}
D_{i_1, i_2} &= 2^{-(j_1+j_2+2)} \left((x_1 - x_2) \frac{\partial \mathcal{U}}{\partial x}(x_5, y_1) - (x_3 - x_4) \frac{\partial \mathcal{U}}{\partial x}(x_6, y_2) \right) \\
\Rightarrow D_{i_1, i_2}^2 &= 2^{-2(j_1+j_2+2)} \left((x_1 - x_2)^2 \left(\frac{\partial \mathcal{U}}{\partial x}(x_5, y_1) \right)^2 + (x_3 - x_4)^2 \left(\frac{\partial \mathcal{U}}{\partial x}(x_6, y_2) \right)^2 \right. \\
&\quad \left. - 2(x_1 - x_2)(x_3 - x_4) \frac{\partial \mathcal{U}}{\partial x}(x_5, y_1) \frac{\partial \mathcal{U}}{\partial x}(x_6, y_2) \right),
\end{aligned}$$

for some $x_5 \in (x_1, x_2)$, $x_6 \in (x_3, x_4)$. Taking modulus on both sides of the above equation, we get

$$\begin{aligned}
\left| D_{i_1, i_2}^2 \right| &\leq 2^{-2(j_1+j_2+2)} \left(|x_1 - x_2|^2 \left| \frac{\partial \mathcal{U}}{\partial x}(x_5, y_1) \right|^2 + |x_3 - x_4|^2 \left| \frac{\partial \mathcal{U}}{\partial x}(x_6, y_2) \right|^2 \right. \\
&\quad \left. + 2|x_1 - x_2||x_3 - x_4| \left| \frac{\partial \mathcal{U}}{\partial x}(x_5, y_1) \right| \left| \frac{\partial \mathcal{U}}{\partial x}(x_6, y_2) \right| \right) \\
&\leq 2^{-2(j_1+j_2+2)} 4\mathcal{M}^2.
\end{aligned}$$

Finally, from (4.6), one obtain

$$\begin{aligned}
\left\| \mathcal{U}_{\text{Exact}}(x, y) - \mathcal{U}_{\text{Numer.}}(x, y) \right\|_{L^2}^2 &\leq \frac{1}{4M_1 M_2} \sum_{i_1=2M_1+1}^{\infty} \sum_{i_2=2M_2+1}^{\infty} \left| D_{i_1, i_2}^2 \right| \\
&\leq \frac{\mathcal{M}^2}{16M_1 M_2} \sum_{j_1=J_1+1}^{\infty} \frac{1}{4^{j_1}} \sum_{j_2=J_2+1}^{\infty} \frac{1}{4^{j_2}} \\
&\leq \frac{\mathcal{M}^2}{144(M_1 M_2)^3}.
\end{aligned}$$

Hence,

$$\left\| \mathcal{U}_{\text{Exact}}(x, y) - \mathcal{U}_{\text{Numer.}}(x, y) \right\|_{L^2} \leq \frac{\mathcal{M}}{12(M_1 M_2)^{3/2}}.$$

This completes the proof. \square

5. Results and discussion

In this section, we consider numerous examples to show the effectiveness and the high accuracy of the proposed $L2-1_\sigma$ method in comparison with the so-called $L1$ method. Several tests are performed and the results are shown in the shape of figures and tables.

Example 5.1. Consider the following time-fractional integro-PDE of the form:

$$\left\{ \begin{array}{l} \partial_t^\alpha \mathcal{U}(x, t) - (1+x) \frac{\partial^2 \mathcal{U}}{\partial x^2} + \mathcal{U}(x, t) + \int_0^t \mathcal{K}(x, t-\xi) \mathcal{U}(x, \xi) d\xi = f(x, t), \quad (x, t) \in [0, 1] \times (0, 1], \\ \text{with initial and boundary conditions:} \\ \mathcal{U}(x, 0) = \sin \pi x \quad \forall x \in [0, 1], \\ \mathcal{U}(0, t) = 0, \quad \mathcal{U}(1, t) = 0 \quad \forall t \in (0, 1], \end{array} \right.$$

where $\alpha \in (0, 1)$. The kernel $\mathcal{K}(x, t-\xi) = (t-\xi) \sin x$ and $f(x, t)$ is given by:

$$f(x, t) = \frac{\Gamma(\alpha+5)}{24} t^4 \sin \pi x + \pi^2 (1+t^{\alpha+4})(1+x) \sin \pi x + (1+t^{\alpha+4}) \sin \pi x + \left(\frac{t^2}{2} + \frac{t^{\alpha+6}}{(\alpha+5)(\alpha+6)} \right) \sin x \sin \pi x.$$

The exact solution for Example 5.1 is $\mathcal{U}(x, t) = (1+t^{\alpha+4}) \sin \pi x$. If $\{\mathcal{U}(x_m, t_n)\}_{m=0, n=0}^{M, N}$ and $\{\mathcal{U}_m^n\}_{m=0, n=0}^{M, N}$ denote the exact and the numerical solution of Example 5.1 by using the proposed scheme (3.9), then the computed error $\widehat{E}_{M, N}$ and the corresponding rate of convergence $\widehat{P}_{M, N}$ are estimated as:

$$\widehat{E}_{M, N} = \max_{(x_m, t_n) \in \Omega_{M, N}} |\mathcal{U}(x_m, t_n) - \mathcal{U}_m^n|, \quad \widehat{P}_{M, N} = \log_2 \left(\frac{\widehat{E}_{M, N}}{\widehat{E}_{2M, 2N}} \right). \quad (5.1)$$

The graphical representation of the exact and the corresponding numerical solution is portrayed in Figure 1(a) and Figure 1(b), respectively with $\alpha = 0.3$ for $M = 32, N = 64$. The surface displayed in Figure 2(a) depicts the maximum error for different values of α for $M = N$. From this representation, it is observed that the error plot decreases as N increases. This proves the convergence of the proposed method. The comparison of the results obtained by the proposed scheme with the results obtained by the $L1$ scheme are shown through log-log plot in Figure 2(b) with $\alpha = 0.7$ for Example 5.1. It can be seen that the straight lines corresponding to the errors and the error bounds are in a parallel position by making an angle with the negative x-axis which is larger than the angle made by the $L1$ scheme. This proves that the $L2-1_\sigma$ scheme gives better accuracy than the $L1$ scheme for solving such fractional-order integro PDEs. The computed error ($\widehat{E}_{M, N}$) and the order of convergence ($\widehat{P}_{M, N}$) are displayed in tabular form in Table 1 for $\alpha = 0.2, 0.5, 0.8$, respectively. The data confirms the second-order convergence of the proposed scheme which satisfies our theoretical analysis shown in Theorem 4.4. The results depicted in Table 2 display the comparison between $L2-1_\sigma$ and $L1$ schemes with $\alpha = 0.1, 0.9$ for Example 5.1. From this illustration, it is clear that the proposed scheme gives second-order accuracy for any values of α whereas, $L1$ scheme exhibits almost first-order accuracy for α tends to 1 (see Remark 1).

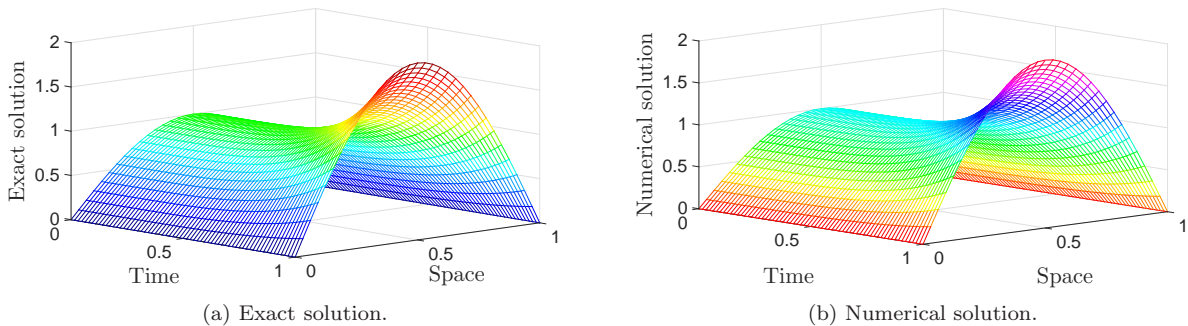
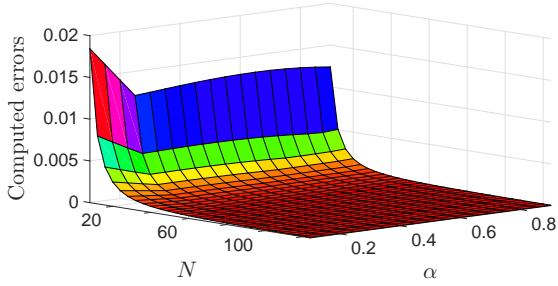
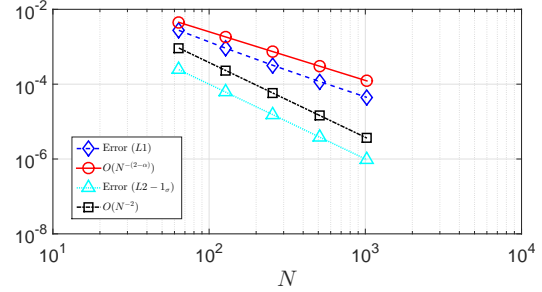


Figure 1. Solutions with $\alpha = 0.3$ and $M = 32, N = 64$ for Example 5.1.



(a) Computed errors.



(b) Log-log plot with $\alpha = 0.7$.

Figure 2. Error and log-log plots for Example 5.1.

Table 1. $\hat{E}_{M,N}$ and $\hat{P}_{M,N}$ by $L2-1_\sigma$ scheme for Example 5.1.

N/M	$\alpha = 0.2$		$\alpha = 0.5$		$\alpha = 0.8$	
	Maximum errors	Rate of convergence	Maximum errors	Rate of convergence	Maximum errors	Rate of convergence
32/16	5.0469e-3	2.0028	4.2082e-3	2.0032	3.4737e-3	2.0010
64/32	1.2592e-3	2.0010	1.0497e-3	2.0009	8.6779e-4	1.9990
128/64	3.1459e-4	2.0004	2.6226e-4	2.0001	2.1710e-4	1.9984
256/128	7.8628e-5	2.0001	6.5560e-5	1.9998	5.4334e-5	1.9982
512/256	1.9655e-5		1.6392e-5		1.3601e-5	

Example 5.2. Let $\alpha \in (0, 1)$. Consider the following test problem:

$$\left\{ \begin{array}{l} \partial_t^\alpha \mathcal{U}(x, t) - \frac{\partial^2 \mathcal{U}}{\partial x^2} + \int_0^t x(t - \xi) \mathcal{U}(x, \xi) d\xi = f(x, t), \quad (x, t) \in [0, 1] \times (0, 1], \\ \text{with initial and boundary conditions:} \\ \mathcal{U}(x, 0) = 0 \quad \forall x \in [0, 1], \\ \mathcal{U}(0, t) = t + t^{\alpha+3}, \quad \mathcal{U}(1, t) = 0 \quad \forall t \in (0, 1], \end{array} \right.$$

where $f(x, t)$ is given by: $f(x, t) = (1 - x^2) \left(\frac{t^{1-\alpha}}{\Gamma(2-\alpha)} + \frac{1}{6} \Gamma(\alpha+4) t^3 \right) + 2(t + t^{\alpha+3}) + x(1 - x^2) \left(\frac{t^3}{6} + \frac{t^{\alpha+5}}{(\alpha+4)(\alpha+5)} \right)$. The exact solution for Example 5.2 is $\mathcal{U}(x, t) = (1 - x^2)(t + t^{\alpha+3})$. The error and the rate of convergence are calculated by the same formula as defined in (5.1).

We display the surface plots of the exact solution and the respective numerical solution in Figure 3 with $\alpha = 0.5$ for $M = 32, N = 64$. The comparison results are shown in Figure 4(a) in terms of maximum error, and in Figure 4(b) based on log-log plot. It is clearly observed that the proposed scheme (3.9) not only gives higher order accuracy (see Figure 4(a)) but also the obtained errors are less (see Figure 4(b)) compared to the $L1$ scheme. The error and the convergence rate are also shown in Table 3 for $\alpha = 0.3, 0.6, 0.9$, respectively based on $L2-1_\sigma$ scheme as well as the $L1$ scheme, by fixing $M = N$. Further, we display the comparison results in Table 4 for $\alpha = 0.2, 0.5, 0.8$, respectively by taking unequal mesh sizes for Example 5.2. In conclusion with the numerical results depicted in Table 3, 4, it is clear that the proposed method gives better accuracy namely second order (see also Note 2) for any values of α , but on the contrary, the $L1$ scheme gives $2 - \alpha$ rate of convergence (see Note 3) for $\alpha \in (0, 1)$, and exhibits a first order convergence rate as α tends to one (see also Remark 1).

Below, we present another example of type (1.1) for which the exact solution is unknown. The double mesh principle [23] is used to calculate the error and the order of convergence as follows: Suppose \mathcal{U}_m^n be the numerical solution for $m = 0, 1, \dots, M$ and $n = 0, 1, \dots, N$. Now consider a fine

Table 2. Comparison of $\hat{E}_{M,N}$ and $\hat{P}_{M,N}$ between $L1$ and $L2-1_\sigma$ schemes for Example 5.1.

α	N/M	$L2-1_\sigma$ scheme		$L1$ scheme	
		Maximum errors	Rate of convergence	Maximum errors	Rate of convergence
0.1	64/32	1.3317e-3	2.0008	1.4125e-3	1.9983
	128/64	3.3275e-4	2.0003	3.5353e-4	1.9978
	256/128	8.3170e-5	2.0001	8.8517e-5	1.9976
	512/256	2.0791e-5	2.0000	2.2167e-5	1.9973
	1024/512	5.1977e-6		5.5519e-6	
0.9	64/32	8.1502e-4	1.9988	5.9369e-3	1.2465
	128/64	2.0393e-4	1.9982	2.5022e-3	1.1855
	256/128	5.1046e-5	1.9980	1.1002e-3	1.1479
	512/256	1.2779e-5	1.9981	4.9648e-4	1.1263
	1024/512	3.1991e-6		2.2743e-4	

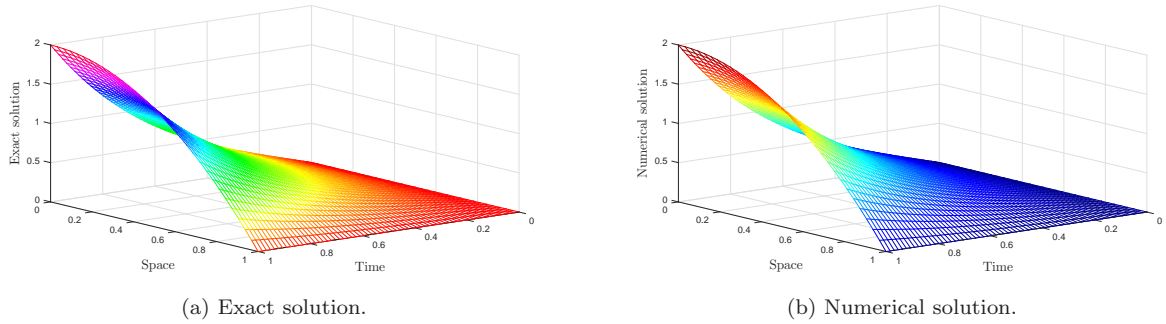


Figure 3. Solutions with $\alpha = 0.5$ and $M = 32, N = 64$ for Example 5.2.

mesh $\{(x_{m/2}, t_{n/2}) \mid m = 0, 1, \dots, 2M \text{ and } n = 0, 1, \dots, 2N\}$, and let $\mathcal{V}_{m/2}^{n/2}$ be the corresponding computed solution by using the same scheme. Then the error and the corresponding convergence rate is estimated as:

$$\tilde{E}_{M,N} := \max_{(x_m, t_n) \in \Omega_{M,N}} |\mathcal{U}_m^n - \mathcal{V}_m^n|, \quad \tilde{P}_{M,N} := \log_2 \left(\frac{\tilde{E}_{M,N}}{\tilde{E}_{2M,2N}} \right). \quad (5.2)$$

Example 5.3. Consider the following fractional order integro PDE:

$$\left\{ \begin{array}{l} \partial_t^\alpha \mathcal{U}(x, t) - \frac{\partial^2 \mathcal{U}}{\partial x^2} + x\mathcal{U}(x, t) + \int_0^t \mathcal{K}(x, t - \xi)\mathcal{U}(x, \xi)d\xi = xt^{4+\alpha}, \quad (x, t) \in [0, 1] \times (0, 1], \\ \text{with initial and boundary conditions:} \\ \mathcal{U}(x, 0) = 0 \quad \forall x \in [0, 1], \\ \mathcal{U}(0, t) = \mathcal{U}(1, t) = 0 \quad \forall t \in (0, 1], \end{array} \right.$$

where $\alpha \in (0, 1)$, and the kernel $\mathcal{K} = e^{x(t-\xi)}$, $\xi \in [0, t]$, $t \in [0, 1]$. We solve the model by using the proposed scheme (3.9) and the results are displayed in the shape of figures and tables. The graphical representation of the numerical solution is displayed in Figure 5 through contour plot (see Figure 5(a)) and surface plot (see Figure 5(b)), respectively. Since the exact solution is unknown, we calculate the error and the rate of convergence by using the formula depicted in (5.2), and the data are tabulated in Table 5 for $\alpha = 0.3, 0.6, 0.9$. One can also see that the obtained rate of convergence is almost second order which confirms the theoretical analysis described in Theorem 4.4.

The following example shows the strong reliability of the wavelet approximation applied on a two-dimensional fractional integro-PDE. The maximum absolute error (L^∞ -error) and the L^2 -error

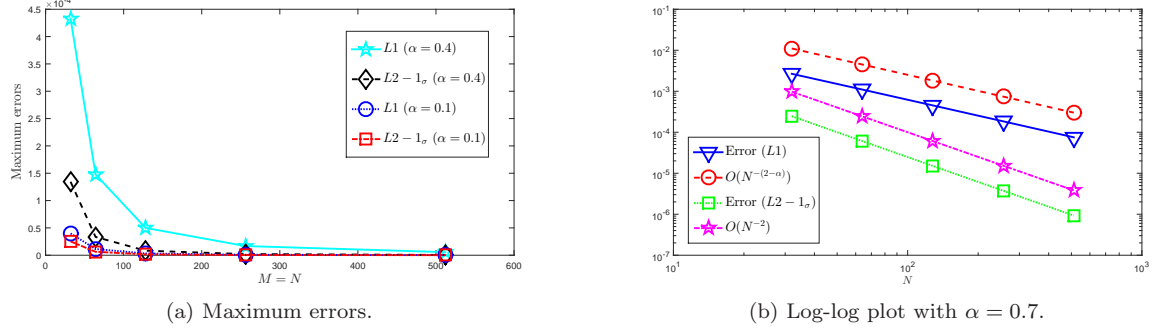


Figure 4. Comparison between $L1$ and $L2-1_\sigma$ schemes for Example 5.2.

Table 3. Comparison of $\hat{E}_{M,N}$ and $\hat{P}_{M,N}$ between $L1$ and $L2-1_\sigma$ schemes for Example 5.2.

α	$N = M$	$L2-1_\sigma$ scheme		$L1$ scheme	
		Maximum errors	Rate of convergence	Maximum errors	Rate of convergence
0.3	32	9.7316e-5	2.0034	2.1852e-4	1.6371
	64	2.4271e-5	2.0036	7.0256e-5	1.6515
	128	6.0525e-6	2.0029	2.2363e-5	1.6623
	256	1.5100e-6	2.0022	7.0654e-6	1.6703
	512	3.7692e-7		2.2199e-6	
0.6	32	2.0888e-4	2.0125	1.4945e-3	1.3694
	64	5.1770e-5	2.0117	5.7843e-4	1.3809
	128	1.2838e-5	2.0100	2.2211e-4	1.3879
	256	3.1874e-6	2.0082	8.4874e-5	1.3922
	512	7.9234e-7		3.2335e-5	
0.9	32	3.2295e-4	2.0117	7.9829e-3	1.0835
	64	8.0085e-5	2.0125	3.7669e-3	1.0914
	128	1.9848e-5	2.0125	1.7679e-3	1.0955
	256	4.9192e-6	2.0121	8.2735e-4	1.0976
	512	1.2196e-6		3.8661e-4	

can be estimated by using the formula defined by:

$$L^\infty\text{-error} := \max_{1 \leq l_1 \leq 2M_1} \max_{1 \leq l_2 \leq 2M_2} \left| \mathcal{U}_{\text{Exact}}(x_{l_1}, y_{l_2}) - \mathcal{U}_{\text{Numer.}}(x_{l_1}, y_{l_2}) \right|,$$

$$L^2\text{-error} := \left(\frac{1}{2M_1 \times 2M_2} \sum_{l_1=1}^{2M_1} \sum_{l_2=1}^{2M_2} \left| \mathcal{U}_{\text{Exact}}(x_{l_1}, y_{l_2}) - \mathcal{U}_{\text{Numer.}}(x_{l_1}, y_{l_2}) \right|^2 \right)^{1/2}.$$

Example 5.4. Consider the following fractional-order two-dimensional integro-PDE:

$$\left\{ \begin{array}{l} \partial_t^\alpha \mathcal{U}(x, y, t) - \frac{\partial^2 \mathcal{U}}{\partial x^2} - \frac{\partial^2 \mathcal{U}}{\partial y^2} + \frac{\partial \mathcal{U}}{\partial x} + \int_0^t xy(t - \xi) \mathcal{U}(x, y, \xi) d\xi = f(x, y, t), \quad (x, y, t) \in \mathcal{G} \times (0, 1], \\ \text{with initial and boundary conditions:} \\ \mathcal{U}(x, y, 0) = xy(x-1)(y-1) \quad \forall (x, y) \in \mathcal{G}, \\ \mathcal{U}(0, y, t) = \mathcal{U}(1, y, t) = 0 \quad \forall (y, t) \in [0, 1] \times (0, 1], \\ \mathcal{U}(x, 0, t) = \mathcal{U}(x, 1, t) = 0 \quad \forall (x, t) \in [0, 1] \times (0, 1], \end{array} \right.$$

Table 4. Comparison of $\widehat{E}_{M,N}$ and $\widehat{P}_{M,N}$ between $L1$ and $L2-1_\sigma$ schemes for Example 5.2.

α	N/M	$L2-1_\sigma$ scheme		$L1$ scheme	
		Maximum errors	Rate of convergence	Maximum errors	Rate of convergence
0.2	32/16	6.0734e-5	2.0006	1.0166e-4	1.7225
	64/32	1.5177e-5	2.0018	3.0805e-5	1.7361
	128/64	3.7896e-6	2.0016	9.2471e-6	1.7466
	256/128	9.4633e-7	2.0012	2.7556e-6	1.7555
	512/256	2.3638e-7		8.1611e-7	
0.5	32/16	1.7163e-4	2.0088	8.1809e-4	1.4617
	64/32	4.2647e-5	2.0085	2.9702e-4	1.4741
	128/64	1.0599e-5	2.0071	1.0691e-4	1.4824
	256/128	2.6368e-6	2.0055	3.8263e-5	1.4878
	512/256	6.5667e-7		1.3643e-5	
0.8	32/16	2.8351e-4	2.0154	4.6544e-3	1.1803
	64/32	7.0123e-5	2.0157	2.0539e-3	1.1890
	128/64	1.7341e-5	2.0146	9.0084e-4	1.1939
	256/128	4.2917e-6	2.0135	3.9378e-4	1.1966
	512/256	1.0629e-6		1.7181e-4	

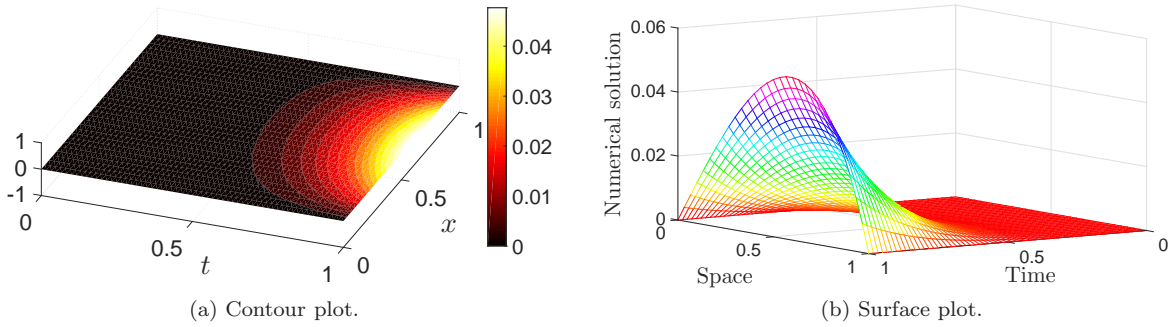


Figure 5. Graphical representation with $\alpha = 0.4$, $M = 30$, $N = 60$ for Example 5.3.

where $\alpha \in (0, 1)$. The source function f is given by:

$$f(x, y, t) = \frac{1}{6} \Gamma(\alpha + 4) xy(x-1)(y-1)t^3 - 2(1 + t^{\alpha+3})(x^2 + y^2 - x - y) \\ + (1 + t^{\alpha+3})(2x-1)(y^2 - y) + \left(\frac{t^2}{2} + \frac{t^{\alpha+5}}{(\alpha+4)(\alpha+5)} \right) x^2 y^2 (x-1)(y-1).$$

The exact solution for Example 5.4 is $\mathcal{U} = (1 + t^{\alpha+3})xy(x-1)(y-1)$. To solve the model, the $L2-1_\sigma$ scheme is used to make it in a semi-discretization form. Then, at each time level, the two-dimensional Haar wavelet is applied to approximate the solution.

The contour plot representation of the exact and numerical solution is shown in Figure 6 for $\alpha = 0.5$, $2M_1 = 2M_2 = 64$ at $t = 0.2$ with $\Delta t = 0.1$. The surface displayed in Figure 7(a) represents the L^∞ -error with $\Delta t = 0.05$ and the maximum level of resolutions $J_1 = J_2 = 3$, for Example 5.4. The corresponding contour plot is displayed in Figure 7(b). Again, the L^2 -error and its corresponding contour plot are graphically represented in Figure 8. One can see that for the given problem, the proposed method gives less error based on the L^2 -error compared to the L^∞ -error, and the comparison is shown in Figure 9. Further, we have tabulated the data of L^∞ -error and L^2 -error in Table 6 for different values of α at $t = 0.2$, 0.6 , and 1 , respectively with $\Delta t = 0.1$, $J_1 = J_2 = 3$.

Table 5. $\tilde{E}_{M,N}$ and $\tilde{P}_{M,N}$ by $L2-1_\sigma$ scheme for Example 5.3.

N/M	$\alpha = 0.3$		$\alpha = 0.6$		$\alpha = 0.9$	
	Maximum errors	Rate of convergence	Maximum errors	Rate of convergence	Maximum errors	Rate of convergence
16/32	1.2692e-4	1.9786	2.2421e-4	1.9872	2.8086e-4	1.9954
32/64	3.2205e-5	1.9907	5.6552e-5	1.9971	7.0437e-5	2.0018
64/128	8.1033e-6	1.9962	1.4166e-5	2.0009	1.7587e-5	2.0037
128/256	2.0312e-6	1.9986	3.5393e-6	2.0023	4.3856e-6	2.0045
256/512	5.0828e-7		8.8345e-7		1.0930e-6	

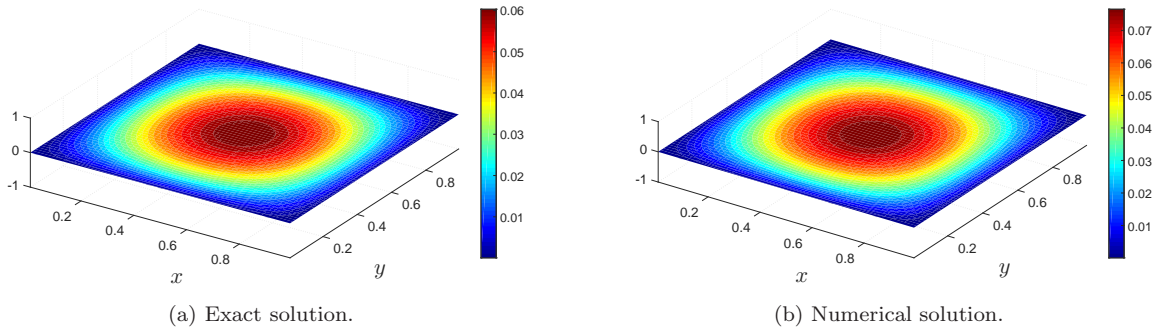


Figure 6. Contour plot representation with $\alpha = 0.5$ and $2M_1 = 2M_2 = 64$ at $t = 0.2$ with $\Delta t = 1/10$ for Example 5.4.

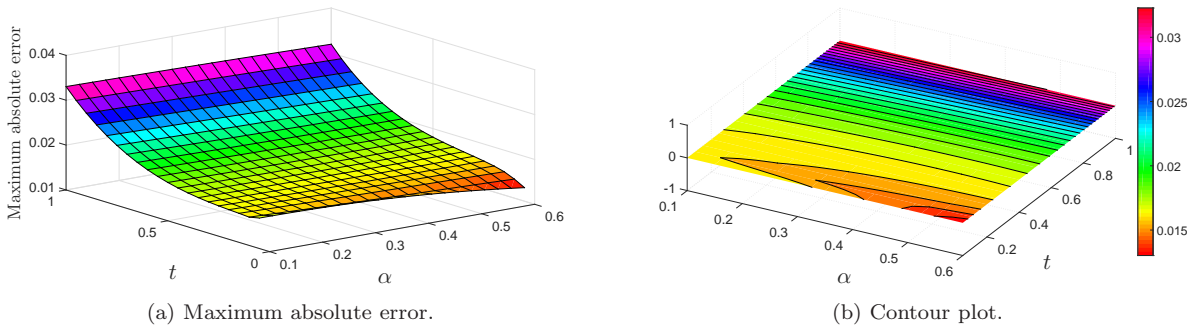


Figure 7. Graphical representation of maximum absolute error with $J_1 = J_2 = 3$ and $\Delta t = 1/20$ for Example 5.4.

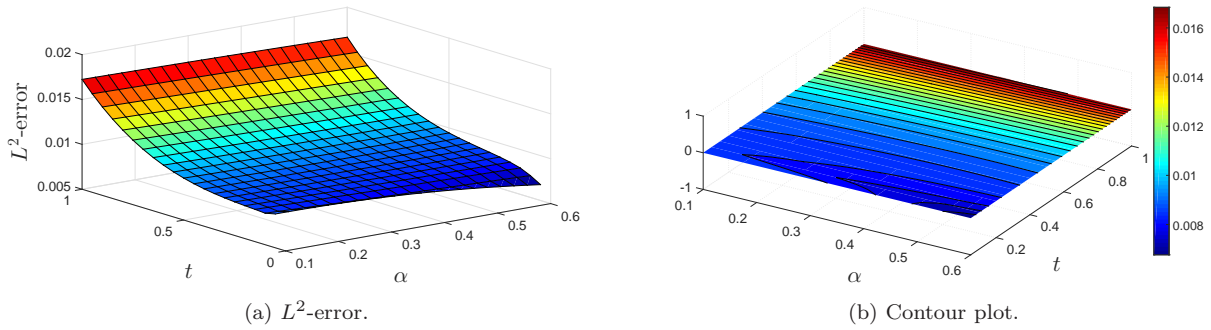


Figure 8. Graphical representation of L^2 -error with $J_1 = J_2 = 3$ and $\Delta t = 1/20$ for Example 5.4.

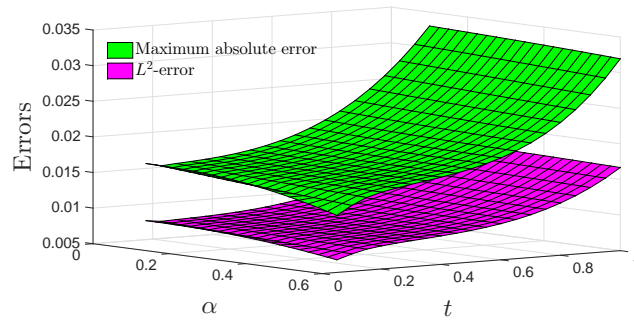


Figure 9. Graphical comparison of maximum absolute error and L^2 -error with $J_1 = J_2 = 3$ and $\Delta t = 1/20$ for Example 5.4.

Table 6. L^∞ -error and L^2 -error with $\Delta t = 1/10$ and $J_1 = J_2 = 3$ at different time levels for Example 5.4.

α	$t = 0.2$		$t = 0.6$		$t = 1$	
	L^∞ -error	L^2 -error	L^∞ -error	L^2 -error	L^∞ -error	L^2 -error
0.3	1.5957e-2	8.3286e-3	1.9485e-2	1.0164e-2	3.2435e-2	1.6920e-2
0.4	1.5761e-2	8.2231e-3	1.9312e-2	1.0073e-2	3.2134e-2	1.6764e-2
0.5	1.5674e-2	8.1710e-3	1.9187e-2	1.0007e-2	3.1808e-2	1.6595e-2
0.6	1.5696e-2	8.1721e-3	1.9116e-2	9.9683e-3	3.1456e-2	1.6412e-2
0.7	1.5780e-2	8.2018e-3	1.9108e-2	9.9610e-3	3.1075e-2	1.6215e-2
0.8	1.5830e-2	8.2103e-3	1.9177e-2	9.9916e-3	3.0664e-2	1.6002e-2

6. Concluding remarks

In the present work, a higher-order numerical approximation based on $L2-1_\sigma$ scheme has been proposed to solve a class of time-fractional integro-PDEs involving Caputo fractional derivatives. The proposed approach is extended to solve a two-dimensional fractional integro-PDE. The wavelet-based numerical approximation is applied to approximate the spatial derivatives at each time level. The stability and convergence analysis of the present method has been proved theoretically as well as computationally. In addition, to show the reliability of the proposed method, the results are compared with the results obtained by the so-called $L1$ scheme. It is proved that the proposed method not only gives higher-order accuracy for solving the given models but also produces less error compared to the $L1$ scheme. The computational results confirm the theoretical arguments.

Declarations

Ethical Approval

The authors follow the basic ethics of the present journal. The present work is neither published nor under consideration at other places.

Funding Details

No funding source is available.

Data Availability Statements

The data sets generated during and/or analyzed during the current study are available from the corresponding author upon reasonable request.

Conflicts of Interest

The authors declare that there are no conflicts of interest.

Informed Consent

On behalf of the authors, Dr. Ratikanta Behera shall be communicating the manuscript.

Authors Information

Sudarshan Santra^a, Ratikanta Behera^a

Affiliations:

^aDepartment of Computational and Data Sciences, Indian Institute of Science, Bangalore, India

Corresponding author:

Correspondence to Ratikanta Behera.

Consent for Publication

All authors provide their consent for publication.

Human and Animal Ethics

Not Applicable.

References

- [1] C. A. Monje, Y. Chen, B. M. Vinagre, D. Xue, V. Feliu, Fractional-order systems and controls, Advances in Industrial Control, Springer, London, 2010.
- [2] M. Roohi, C. Zhang, Y. Chen, Adaptive model-free synchronization of different fractional-order neural networks with an application in cryptography, Nonlinear Dynamics 100 (4) (2020) 3979–4001.
- [3] V. Mehandiratta, M. Mehra, G. Leugering, An approach based on Haar wavelet for the approximation of fractional calculus with application to initial and boundary value problems, Math. Methods Appl. Sci. 44 (4) (2021) 3195–3213. doi:10.1002/mma.6800.
- [4] A. Golbabai, O. Nikan, T. Nikazad, Numerical analysis of time fractional Black-Scholes European option pricing model arising in financial market, Comput. Appl. Math. 38 (4) (2019) Paper No. 173, 24. doi:10.1007/s40314-019-0957-7.

- [5] M. A. Ichou, H. El Amri, A. Ezziani, On existence and uniqueness of solution for space-time fractional Zener model, *Acta Appl. Math.* 170 (2020) 593–609. doi:10.1007/s10440-020-00348-4.
- [6] K. S. Miller, B. Ross, An introduction to the fractional calculus and fractional differential equations, A Wiley-Interscience Publication, John Wiley & Sons, Inc., New York, 1993.
- [7] H. Chen, F. Holland, M. Stynes, An analysis of the Grünwald-Letnikov scheme for initial-value problems with weakly singular solutions, *Appl. Numer. Math.* 139 (2019) 52–61. doi:10.1016/j.apnum.2019.01.004.
- [8] S. Santra, J. Mohapatra, Analysis of a finite difference method based on L1 discretization for solving multi-term fractional differential equation involving weak singularity, *Math. Methods Appl. Sci.* 45 (11) (2022) 6677–6690. doi:10.1002/mma.8199.
- [9] S. Santra, A. Panda, J. Mohapatra, A novel approach for solving multi-term time fractional Volterra-Fredholm partial integro-differential equations, *J. Appl. Math. Comput.* 68 (5) (2022) 3545–3563. doi:10.1007/s12190-021-01675-x.
- [10] S. Abbasbandy, M. S. Hashemi, I. Hashim, On convergence of homotopy analysis method and its application to fractional integro-differential equations, *Quaest. Math.* 36 (1) (2013) 93–105. doi:10.2989/16073606.2013.780336.
- [11] A. A. Hamoud, K. P. Ghadle, Modified Laplace decomposition method for fractional Volterra-Fredholm integro-differential equations, *J. Math. Model.* 6 (1) (2018) 91–104. doi:10.15393/j3.art.2018.4350.
- [12] A. Babaei, S. Banihashemi, C. Cattani, An efficient numerical approach to solve a class of variable-order fractional integro-partial differential equations, *Numer. Methods Partial Differential Equations* 37 (1) (2021) 674–689. doi:10.1002/num.22546.
- [13] Y.-n. Zhang, Z.-z. Sun, H.-l. Liao, Finite difference methods for the time fractional diffusion equation on non-uniform meshes, *J. Comput. Phys.* 265 (2014) 195–210. doi:10.1016/j.jcp.2014.02.008.
- [14] M. Dehghan, M. Abbaszadeh, A Legendre spectral element method (SEM) based on the modified bases for solving neutral delay distributed-order fractional damped diffusion-wave equation, *Math. Methods Appl. Sci.* 41 (9) (2018) 3476–3494. doi:10.1002/mma.4839.
- [15] R. Behera, M. Mehra, A dynamic adaptive wavelet method for solution of the Schrodinger equation, *J. Multiscale Model.* 6 (1) (2015) 1450001, 22. doi:10.1142/S1756973714500012.
- [16] R. Behera, M. Mehra, N. K.-R. Kevlahan, Multilevel approximation of the gradient operator on an adaptive spherical geodesic grid, *Adv. Comput. Math.* 41 (3) (2015) 663–689. doi:10.1007/s10444-014-9382-z.
- [17] K. Schneider, O. V. Vasilyev, Wavelet methods in computational fluid dynamics, in: *Annual review of fluid mechanics*. Vol. 42, Vol. 42 of *Annu. Rev. Fluid Mech.*, Annual Reviews, Palo Alto, CA, 2010, pp. 473–503. doi:10.1146/annurev-fluid-121108-145637.
- [18] N. Pervaiz, I. Aziz, Haar wavelet approximation for the solution of cubic nonlinear Schrodinger equations, *Phys. A* 545 (2020) 123738, 17. doi:10.1016/j.physa.2019.123738.
- [19] S. ul Islam, I. Aziz, F. Haq, A comparative study of numerical integration based on Haar wavelets and hybrid functions, *Comput. Math. Appl.* 59 (6) (2010) 2026–2036. doi:10.1016/j.camwa.2009.12.005.
- [20] D. Baleanu, K. Diethelm, E. Scalas, J. J. Trujillo, *Fractional calculus: Models and numerical methods*, Vol. 5 of *Series on Complexity, Nonlinearity and Chaos*, World Scientific Publishing Co. Pte. Ltd., Hackensack, NJ, 2017.
- [21] S. Santra, J. Mohapatra, A novel finite difference technique with error estimate for time fractional partial integro-differential equation of Volterra type, *J. Comput. Appl. Math.* 400 (2022) Paper No. 113746, 13. doi:10.1016/j.cam.2021.113746.
- [22] J. L. Gracia, E. O’Riordan, M. Stynes, Convergence in positive time for a finite difference method applied to a fractional convection-diffusion problem, *Comput. Methods Appl. Math.* 18 (1) (2018) 33–42. doi:10.1515/cmam-2017-0019.
- [23] S. Santra, J. Mohapatra, Analysis of the L1 scheme for a time fractional parabolic-elliptic problem involving weak singularity, *Math. Methods Appl. Sci.* 44 (2) (2021) 1529–1541. doi:10.1002/mma.6850.
- [24] M. Stynes, E. O’Riordan, J. L. Gracia, Error analysis of a finite difference method on graded meshes for a time-fractional diffusion equation, *SIAM J. Numer. Anal.* 55 (2) (2017) 1057–1079.

doi:10.1137/16M1082329.

- [25] G.-h. Gao, Z.-z. Sun, Y.-n. Zhang, A finite difference scheme for fractional sub-diffusion equations on an unbounded domain using artificial boundary conditions, *J. Comput. Phys.* 231 (7) (2012) 2865–2879. doi:10.1016/j.jcp.2011.12.028.
- [26] G.-h. Gao, Z.-z. Sun, H.-w. Zhang, A new fractional numerical differentiation formula to approximate the Caputo fractional derivative and its applications, *J. Comput. Phys.* 259 (2014) 33–50. doi:10.1016/j.jcp.2013.11.017.
- [27] A. A. Alikhanov, A new difference scheme for the time fractional diffusion equation, *J. Comput. Phys.* 280 (2015) 424–438. doi:10.1016/j.jcp.2014.09.031.
- [28] B. Guo, X. Pu, F. Huang, *Fractional partial differential equations and their numerical solutions*, World Scientific Publishing Co. Pte. Ltd., Hackensack, NJ, 2015. doi:10.1142/9543.
- [29] I. Podlubny, *Fractional differential equations: An introduction to fractional derivatives, fractional differential equations, to methods of their solution and some of their applications*, Vol. 198 of *Mathematics in Science and Engineering*, Academic Press, Inc., San Diego, CA, 1999.
- [30] H. Sun, W. Chen, Y. Chen, Variable-order fractional differential operators in anomalous diffusion modeling, *Physica A: Statistical Mechanics and its Applications* 388 (21) (2009) 4586–4592.
- [31] R. Metzler, J. Klafter, The random walk’s guide to anomalous diffusion: a fractional dynamics approach, *Phys. Rep.* 339 (1) (2000) 77. doi:10.1016/S0370-1573(00)00070-3.
- [32] S. Konjik, L. Oparnica, D. Zorica, Waves in fractional Zener type viscoelastic media, *J. Math. Anal. Appl.* 365 (1) (2010) 259–268. doi:10.1016/j.jmaa.2009.10.043.
- [33] E. Kreyszig, *Introductory functional analysis with applications*, Wiley Classics Library, John Wiley & Sons, Inc., New York, 1989.
- [34] W. Rudin, *Principles of mathematical analysis*, 3rd Edition, International Series in Pure and Applied Mathematics, McGraw-Hill Book Co., New York-Auckland-Düsseldorf, 1976.
- [35] J. Schauder, Der fixpunktsatz in funktionalräumen, *Studia Mathematica* 2 (1) (1930) 171–180.
- [36] A. Haar, Zur Theorie der orthogonalen Funktionensysteme, *Math. Ann.* 69 (3) (1910) 331–371. doi:10.1007/BF01456326.
- [37] S. ul Islam, I. Aziz, B. Šarler, The numerical solution of second-order boundary-value problems by collocation method with the Haar wavelets, *Math. Comput. Modelling* 52 (9-10) (2010) 1577–1590. doi:10.1016/j.mcm.2010.06.023.
- [38] Y. Lin, C. Xu, Finite difference/spectral approximations for the time fractional diffusion equation, *J. Comput. Phys.* 225 (2) (2007) 1533–1552. doi:10.1016/j.jcp.2007.02.001.
- [39] Z.-z. Sun, X. Wu, A fully discrete difference scheme for a diffusion-wave system, *Appl. Numer. Math.* 56 (2) (2006) 193–209. doi:10.1016/j.apnum.2005.03.003.
- [40] L. Wang, Y. Ma, Z. Meng, Haar wavelet method for solving fractional partial differential equations numerically, *Appl. Math. Comput.* 227 (2014) 66–76. doi:10.1016/j.amc.2013.11.004.